MNRAS **000**, 1–4 (2017) Preprint 29 March 2018 Compiled using MNRAS LATEX style file v3.0

APPENDIX: An Iwasawa-Taniguchi Effect for Compton-thick AGN

Peter G. Boorman,[1]★ Poshak Gandhi,[1] Mislav Baloković,[2,3] Murray Brightman,[2] Fiona Harrison,[2] Claudio Ricci[4,5,6,7] and Daniel Stern[8]

[1] *Department of Physics & Astronomy, Faculty of Physical Sciences and Engineering, University of Southampton, Southampton, SO17 1BJ, UK*
[2] *Cahill Center for Astronomy and Astrophysics, California Institute of Technology, Pasadena, CA 91125, USA*
[3] *Harvard-Smithsonian Center for Astrophysics, 60 Garden Street, Cambridge, MA 02138, USA*
[4] *Instituto de Astrofísica, Facultad de Física, Pontificia Universidad Católica de Chile, Casilla 306, Santiago 22, Chile*
[5] *Núcleo de Astronomía de la Facultad de Ingeniería, Universidad Diego Portales, Av. Ejército Libertador 441, Santiago, Chile*
[6] *Kavli Institute for Astronomy and Astrophysics, Peking University, Beijing 100871, China*
[7] *Chinese Academy of Sciences South America Center for Astronomy and China-Chile Joint Center for Astronomy, Camino El Observatorio 1515, Las Condes, Santiago, Chile*
[8] *Jet Propulsion Laboratory, California Institute of Technology, Pasadena, CA 91109, USA*

Accepted XXX. Received YYY; in original form ZZZ

REFERENCES

Asmus D., Gandhi P., Hönig S. F., Smette A., Duschl W. J., 2015, MNRAS, 454, 766
Gandhi P., et al., 2013, ApJ, 773, 51
Gandhi P., et al., 2014, ApJ, 792, 117
Ricci C., Ueda Y., Koss M. J., Trakhtenbrot B., Bauer F. E., Gandhi P., 2015, ApJ, 815, L13

All spectra presented here are plotted with energies in the source observed frame on the lower axis, with the source rest-frame energy shown on the upper axis. Sources with an additional `apec` component included in the spectral fit are shown with a corresponding label in their legend.

The grouping used is annotated on each plot and has one of two possibilities:

(i) Binning by a minimum number of counts per bin.
(ii) Binning to have a minimum S/N ratio in each bin.

All sources were fitted with a simplified phenomenological model consisting of photoelectric absorption acting on a composite powerlaw (Γ, the photon index of the powerlaw was assigned to 1.4 for all cases) plus a narrow Gaussian of FWHM $\approx 2\,\mathrm{eV}$ ($\sigma = 1\,\mathrm{eV}$), modelling the observed continuum and narrow core of the Fe Kα fluorescence line, respectively. See Section 3.3 for further details on the spectral model adopted. The corresponding confidence contours shown (where applicable) in the top right panel illustrate a delta statistic of +2.30 to represent the 1-σ (68%) confidence level for two interesting parameters★

All spectra shown feature the spectral fit to the data and the DEL for the fit in the top and bottom panels, respectively. DEL is defined as the (data − model)/error.

APPENDIX A: SOURCES EXCLUDED

NuSTAR data was not publicly available for 19/55 low redshift sources from the *Neil Gehrels Swift*/BAT sample of Ricci et al. (2015), and so were excluded from this work. See Section 2.2 for more information. This excluded ESO 565-G019, which is in the Gandhi et al. (2014) bona-fide Compton-thick AGN sample, and has been studied individually in Gandhi et al. (2013) with *Suzaku* data.

In addition, our own analysis of the archival archival XMM-*Newton* EPIC/PN spectrum as compared to the more recent *NuSTAR* FPMA & FPMB spectra strongly indicated a changing-look AGN scenario for NGC 4102 and NGC 4939. These sources were thus excluded since changing-look AGN could adhere to variable obscuration effects.

Finally, 5 sources had observed rest-frame 2 - 10 keV fluxes in agreement with the interpolated rest-frame 12 μm flux, predicted from the relation presented in Asmus et al. (2015). These 5 sources were ruled out from our sample, and their spectra are shown in Figure A1.

★ https://heasarc.gsfc.nasa.gov/xanadu/xspec/manual/XSappendixStatistics.html

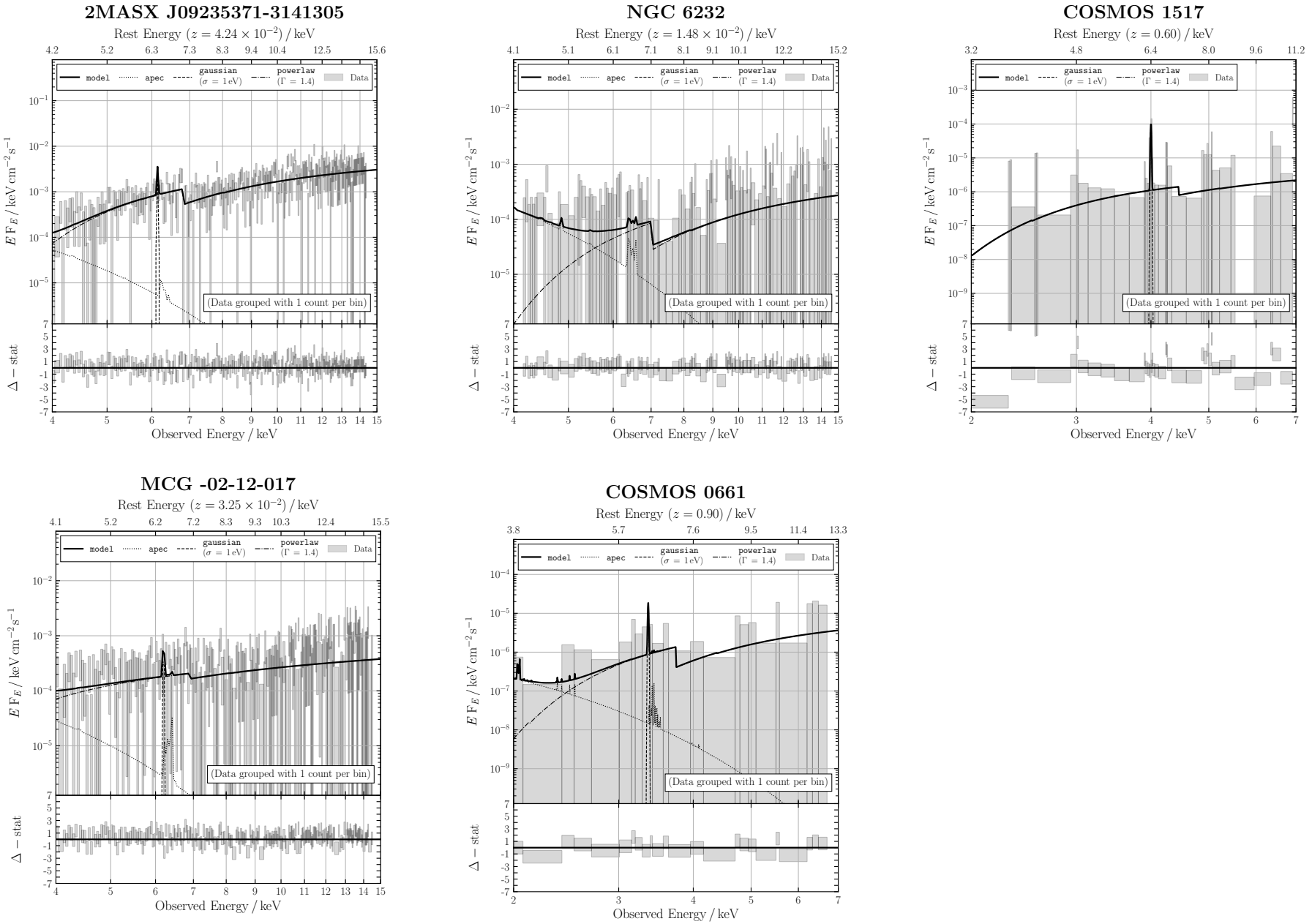

Figure A1. Spectra of the 5 sources ruled out in our analysis due to an agreement with the Asmus et al. (2015) correlation between observed X-ray and mid-infrared luminosity, which can infer less than Compton-thick obscuration. For details of the spectrum, see the description at the start of the Appendix. The top and bottom panels show the spectral fit to the data and the DEL for the fit, respectively. DEL is defined as the (data − model)/error.

APPENDIX B: SOURCES INCLUDED

Here we include individual spectra and equivalent width (EW) contours for the sources we derive EWs for ourselves. The sources are ordered in ascending 12μm luminosity, as in Table 1 of the paper. We used the limit derived from best-fit parameters for 3 sources that the contour method did not provide a reasonable constraint for. These sources are: COSMOS0581, COSMOS 0987 and CDFS 460. Furthermore, due to an unphysical EW determined for CDFS 443, CDFS 454 and COSMOS 2180, we fixed the EW for these sources to be < 5 keV.

The upper right panel for each source figure indicates the contour plot for the EW, with the grid best-fit values shown as faint grey points. Statistical details of the spectral fit are tabulated in the bottom right panel of each source figure. All uncertainties shown from the intersection of the horizontal black line with the solid line contour correspond to the 68% confidence level for two interesting parameters.

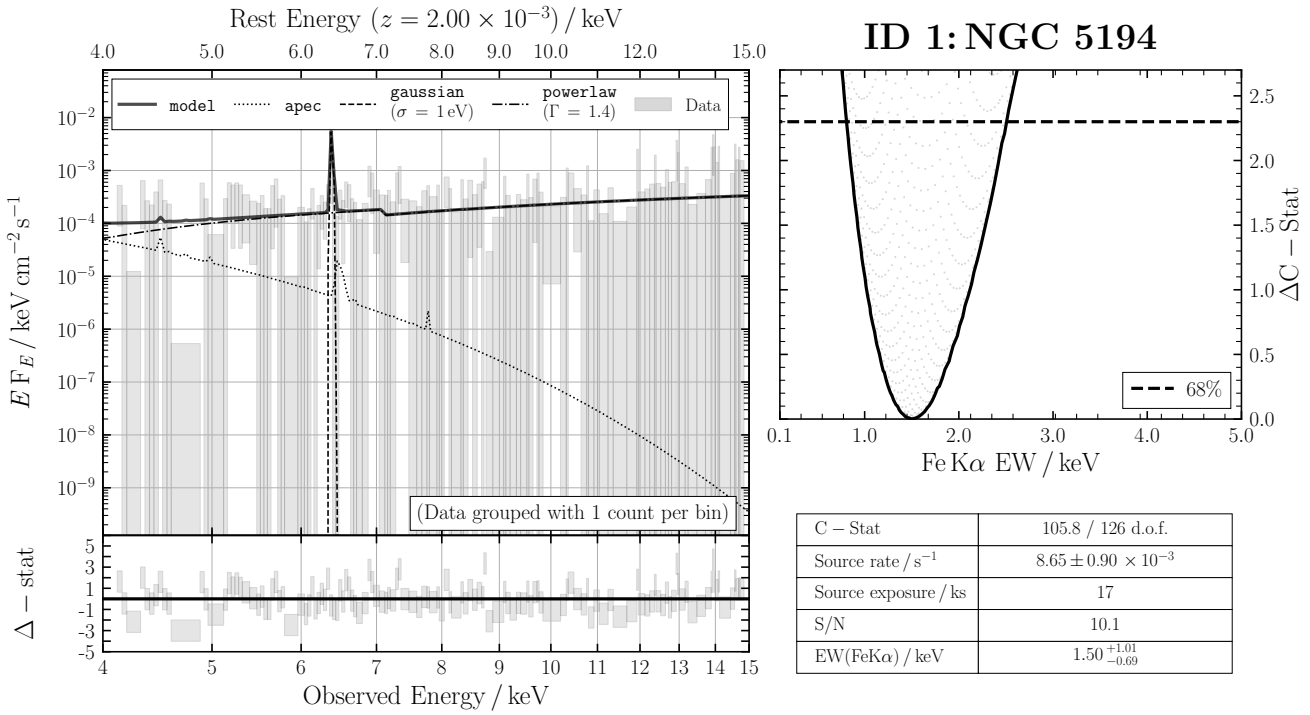

C − Stat	105.8 / 126 d.o.f.
Source rate / s^{-1}	$8.65 \pm 0.90 \times 10^{-3}$
Source exposure / ks	17
S/N	10.1
EW(FeKα) / keV	$1.50^{+1.01}_{-0.69}$

Figure B1. ID 1: NGC 5194

This paper has been typeset from a TEX/LATEX file prepared by the author.

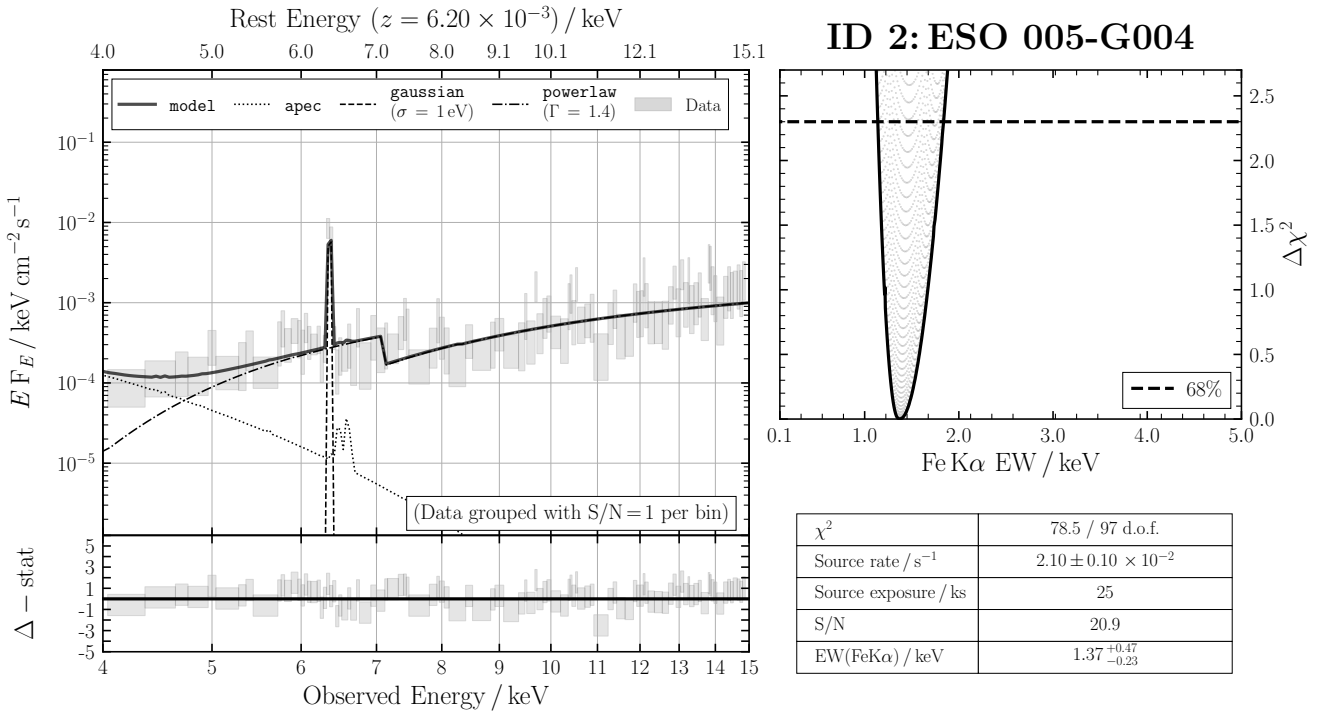

χ^2	78.5 / 97 d.o.f.
Source rate / s^{-1}	$2.10 \pm 0.10 \times 10^{-2}$
Source exposure / ks	25
S/N	20.9
EW(FeKα) / keV	$1.37^{+0.47}_{-0.23}$

Figure B2. ID 2: ESO 005-G004

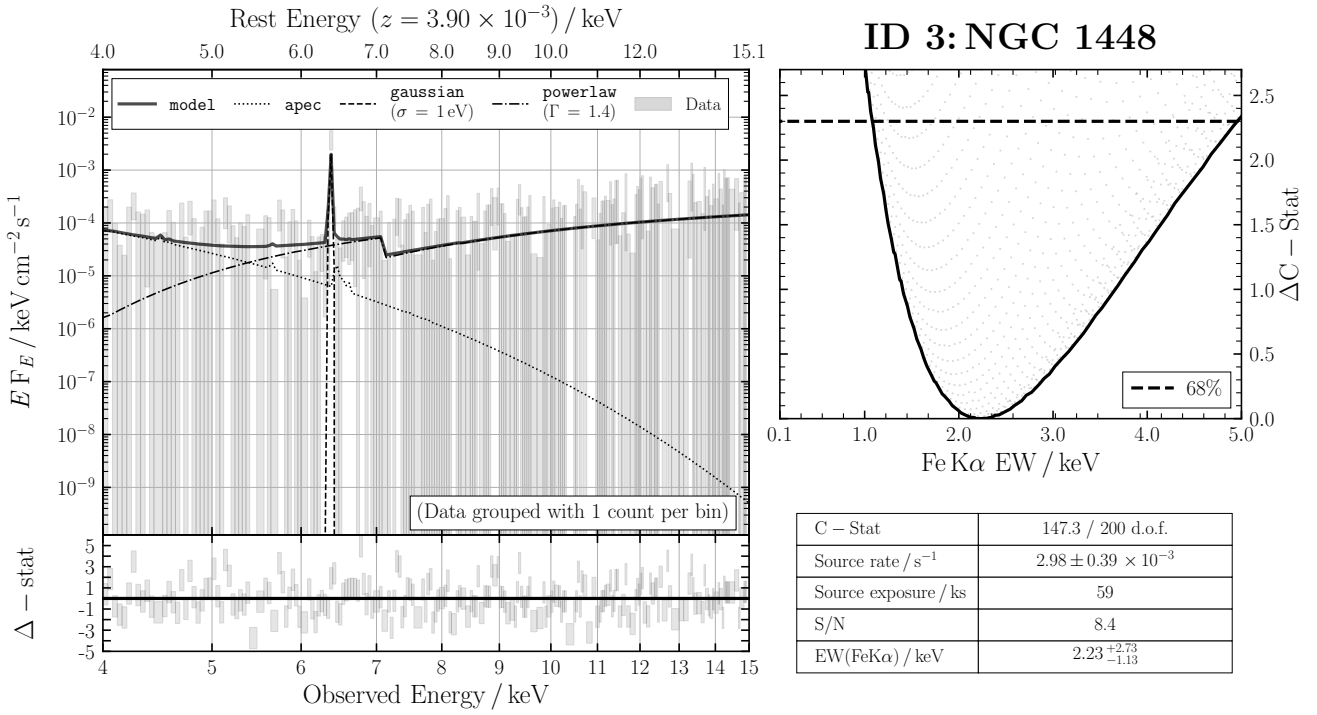

C − Stat	147.3 / 200 d.o.f.
Source rate / s^{-1}	$2.98 \pm 0.39 \times 10^{-3}$
Source exposure / ks	59
S/N	8.4
EW(FeKα) / keV	$2.23^{+2.73}_{-1.13}$

Figure B3. ID 3: NGC 1448

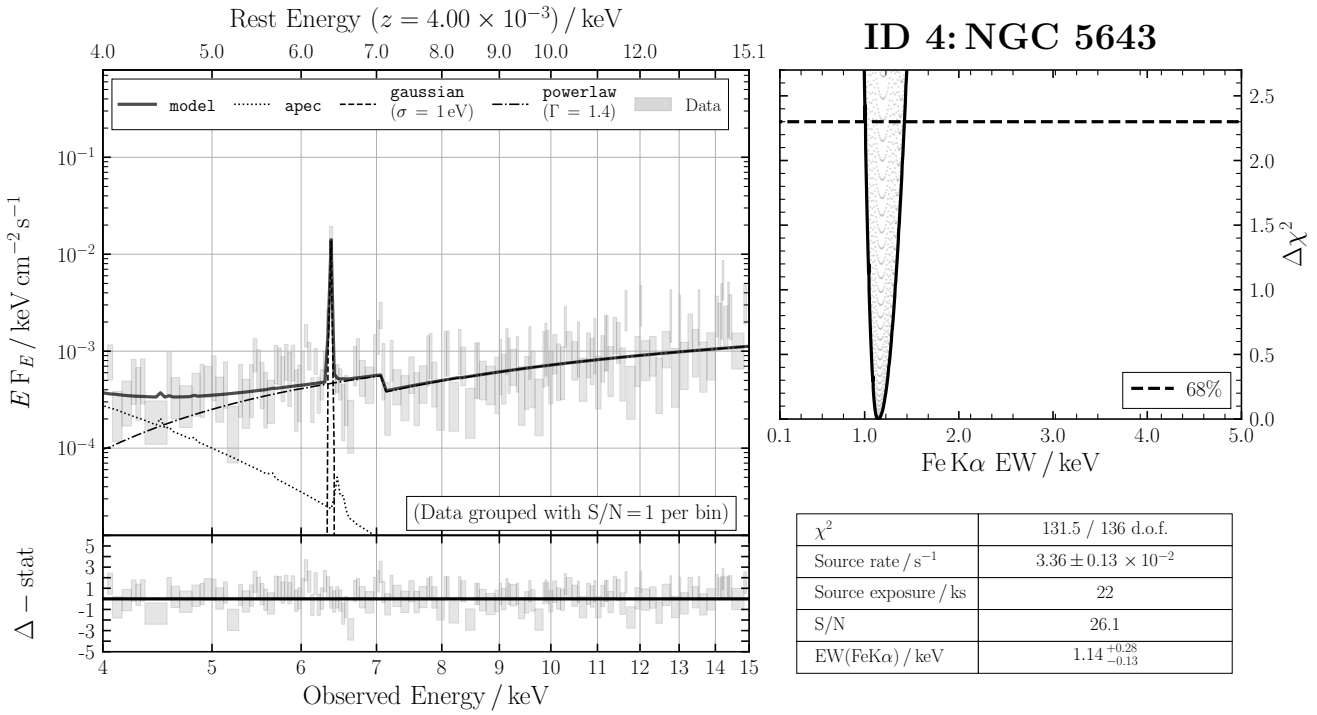

χ^2	131.5 / 136 d.o.f.
Source rate / s^{-1}	$3.36 \pm 0.13 \times 10^{-2}$
Source exposure / ks	22
S/N	26.1
EW(FeKα) / keV	$1.14^{+0.28}_{-0.13}$

Figure B4. ID 4: NGC 5643

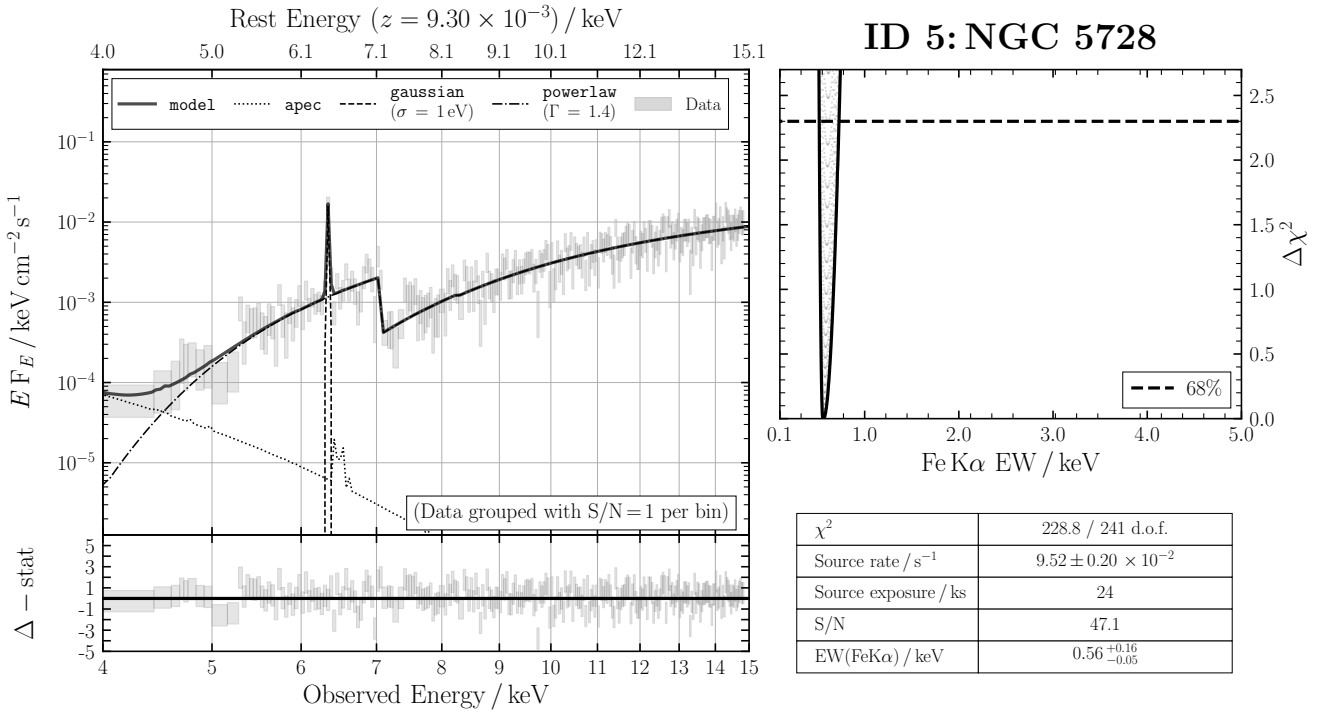

χ^2	228.8 / 241 d.o.f.
Source rate / s^{-1}	$9.52 \pm 0.20 \times 10^{-2}$
Source exposure / ks	24
S/N	47.1
EW(FeKα) / keV	$0.56^{+0.16}_{-0.05}$

Figure B5. ID 5: NGC 5728

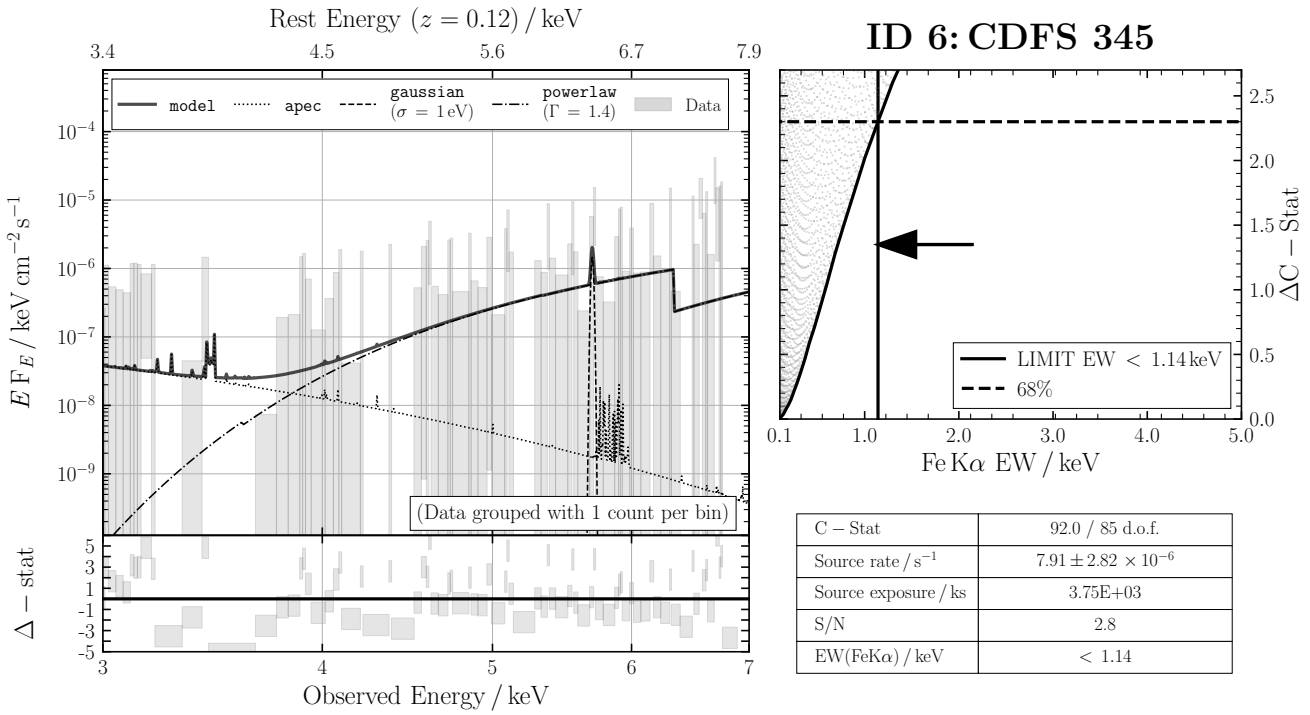

C − Stat	92.0 / 85 d.o.f.
Source rate / s^{-1}	$7.91 \pm 2.82 \times 10^{-6}$
Source exposure / ks	3.75E+03
S/N	2.8
EW(FeKα) / keV	< 1.14

Figure B6. ID 6: CDFS 345

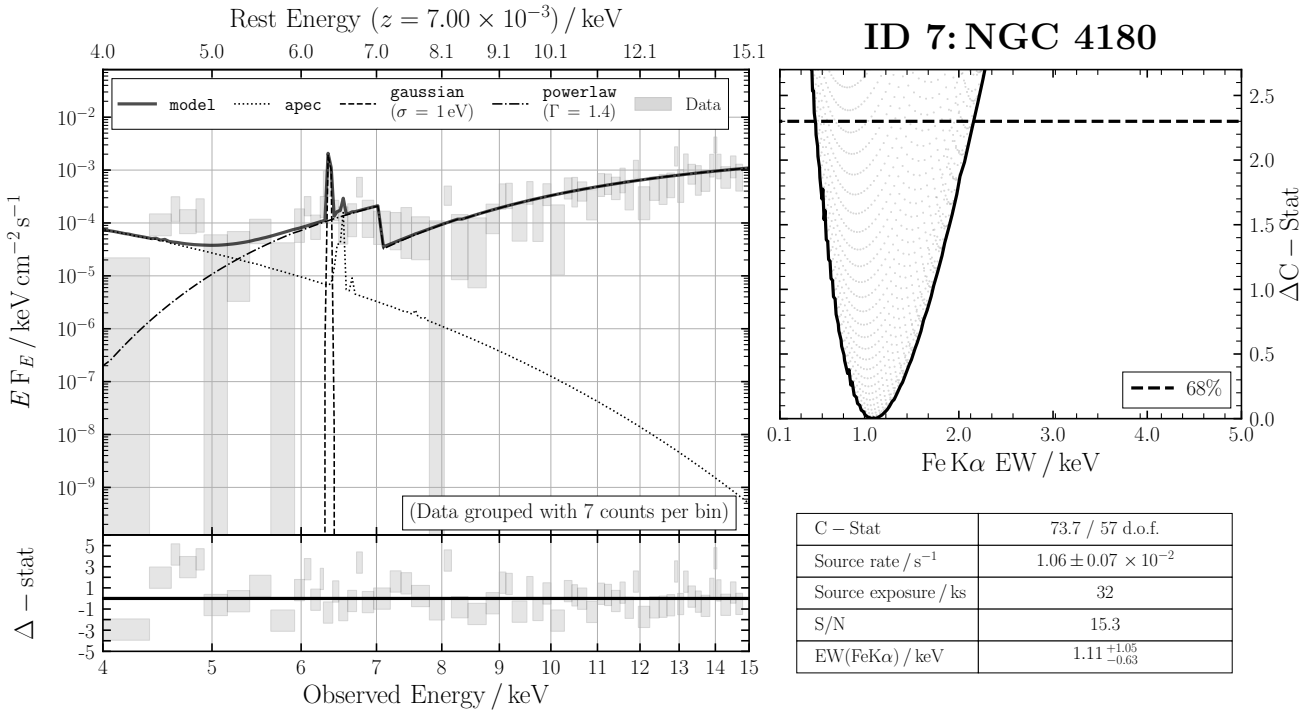

C − Stat	73.7 / 57 d.o.f.
Source rate / s^{-1}	$1.06 \pm 0.07 \times 10^{-2}$
Source exposure / ks	32
S/N	15.3
EW(FeKα) / keV	$1.11^{+1.05}_{-0.63}$

Figure B7. ID 7: NGC 4180

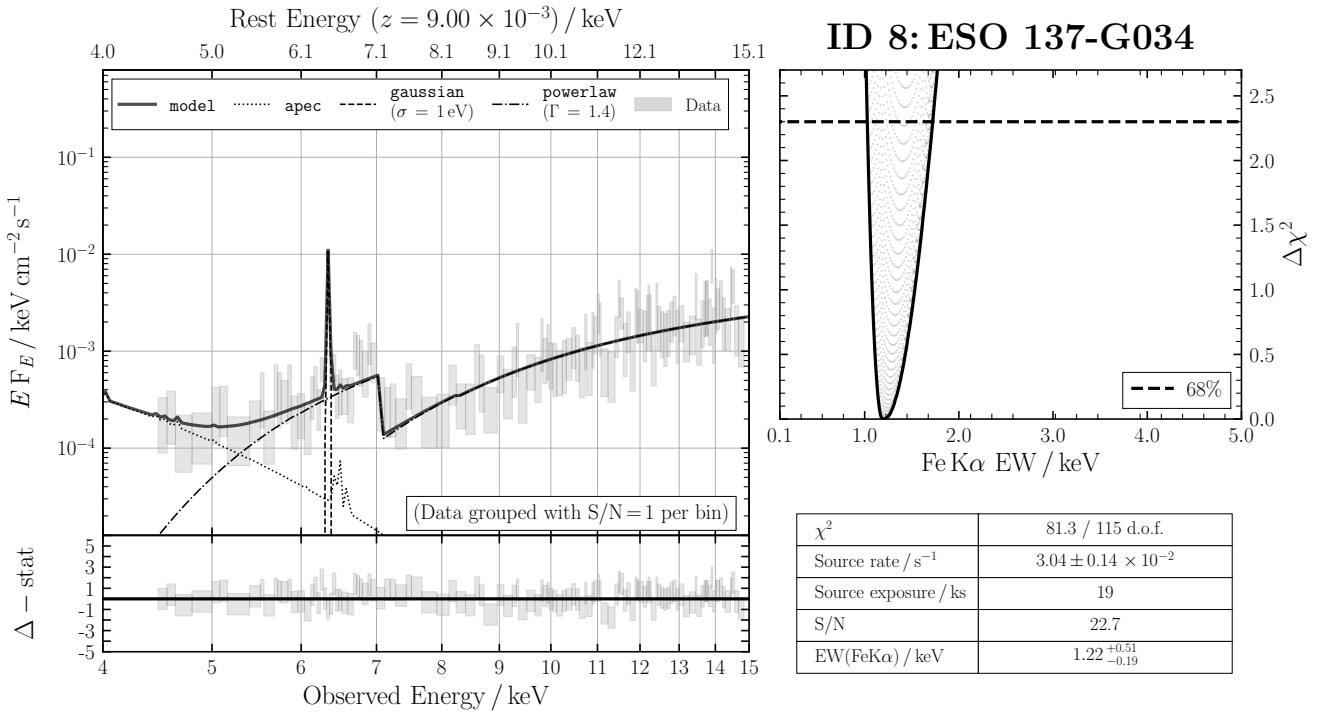

χ^2	81.3 / 115 d.o.f.
Source rate / s^{-1}	$3.04 \pm 0.14 \times 10^{-2}$
Source exposure / ks	19
S/N	22.7
EW(FeKα) / keV	$1.22^{+0.51}_{-0.19}$

Figure B8. ID 8: ESO 137-G034

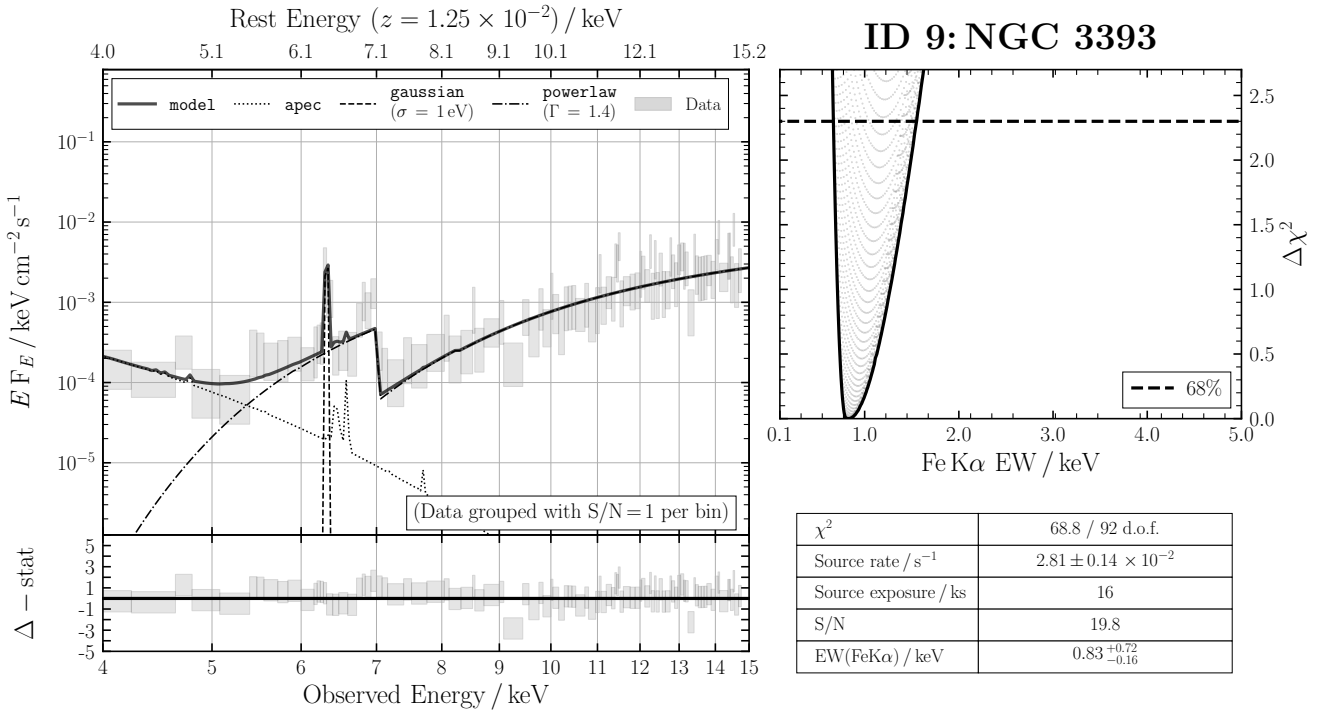

χ^2	68.8 / 92 d.o.f.
Source rate / s^{-1}	$2.81 \pm 0.14 \times 10^{-2}$
Source exposure / ks	16
S/N	19.8
EW(FeKα) / keV	$0.83^{+0.72}_{-0.16}$

Figure B9. ID 9: NGC 3393

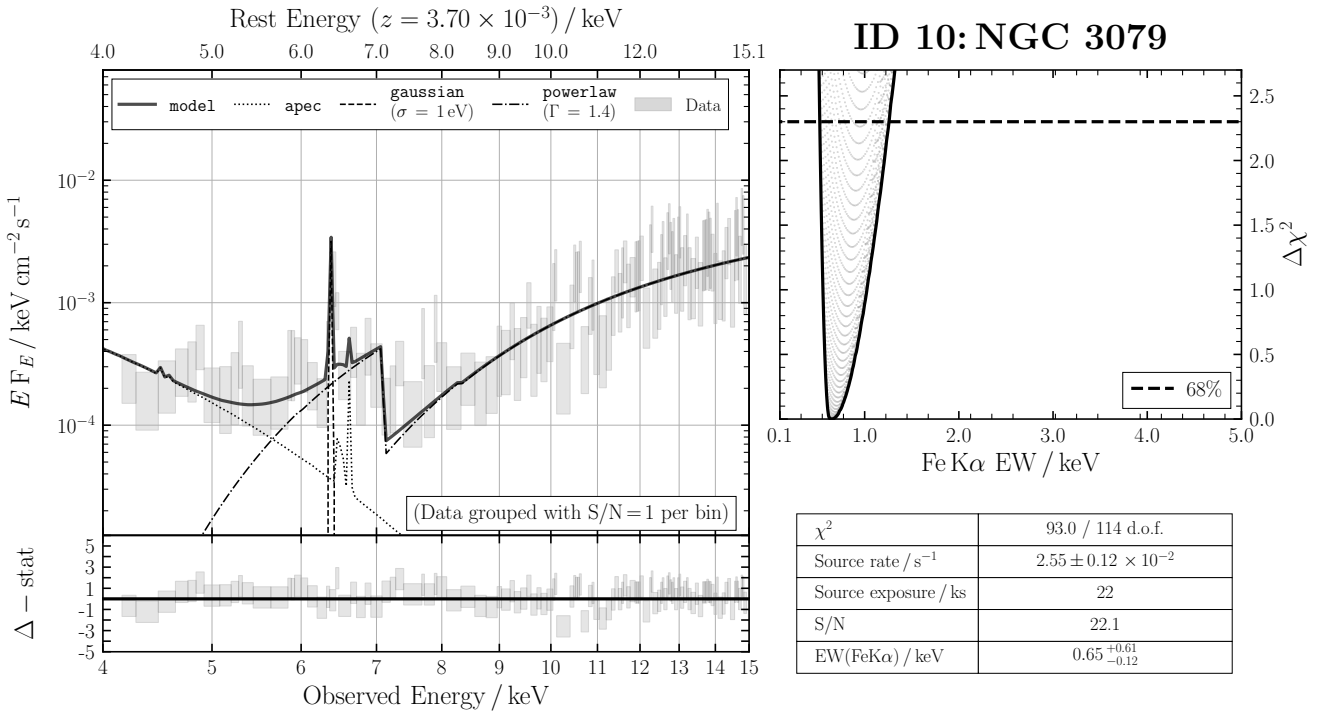

χ^2	93.0 / 114 d.o.f.
Source rate / s^{-1}	$2.55 \pm 0.12 \times 10^{-2}$
Source exposure / ks	22
S/N	22.1
EW(FeKα) / keV	$0.65^{+0.61}_{-0.12}$

Figure B10. ID 10: NGC 3079

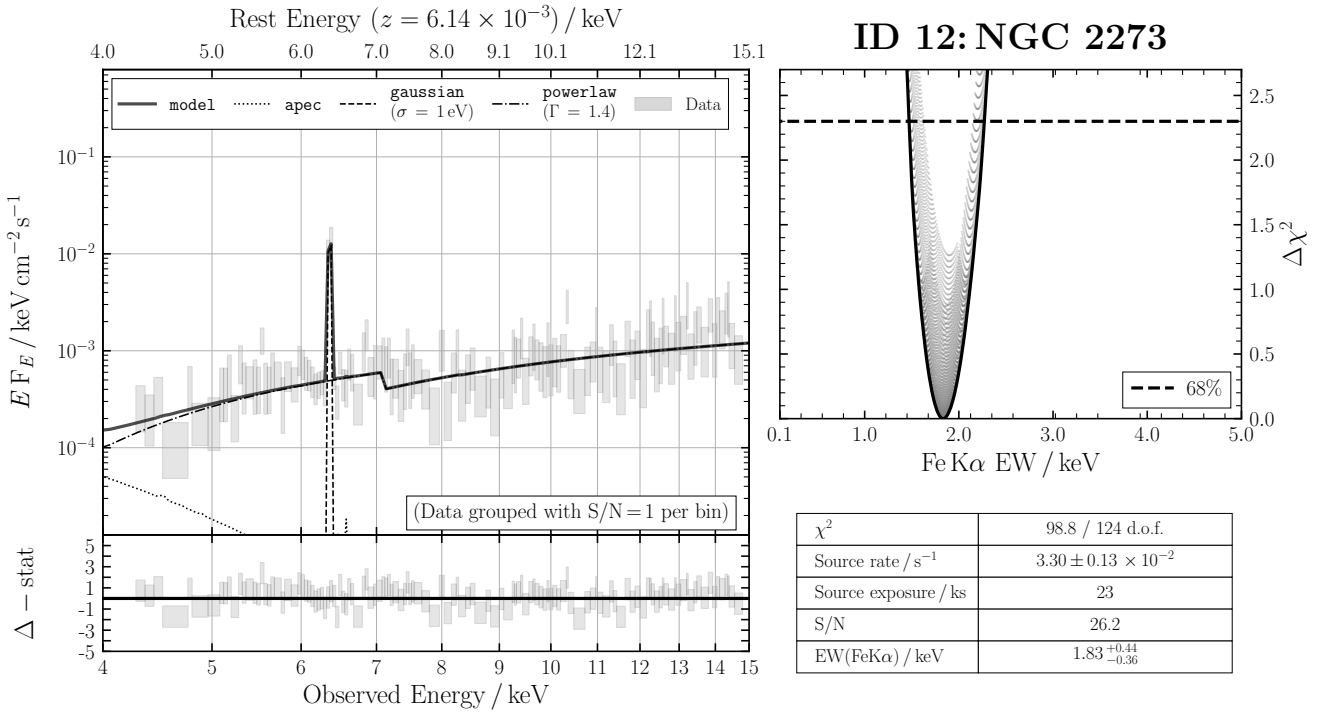

χ^2	98.8 / 124 d.o.f.
Source rate / s^{-1}	$3.30 \pm 0.13 \times 10^{-2}$
Source exposure / ks	23
S/N	26.2
EW(FeKα) / keV	$1.83^{+0.44}_{-0.36}$

Figure B11. ID 12: NGC 2273

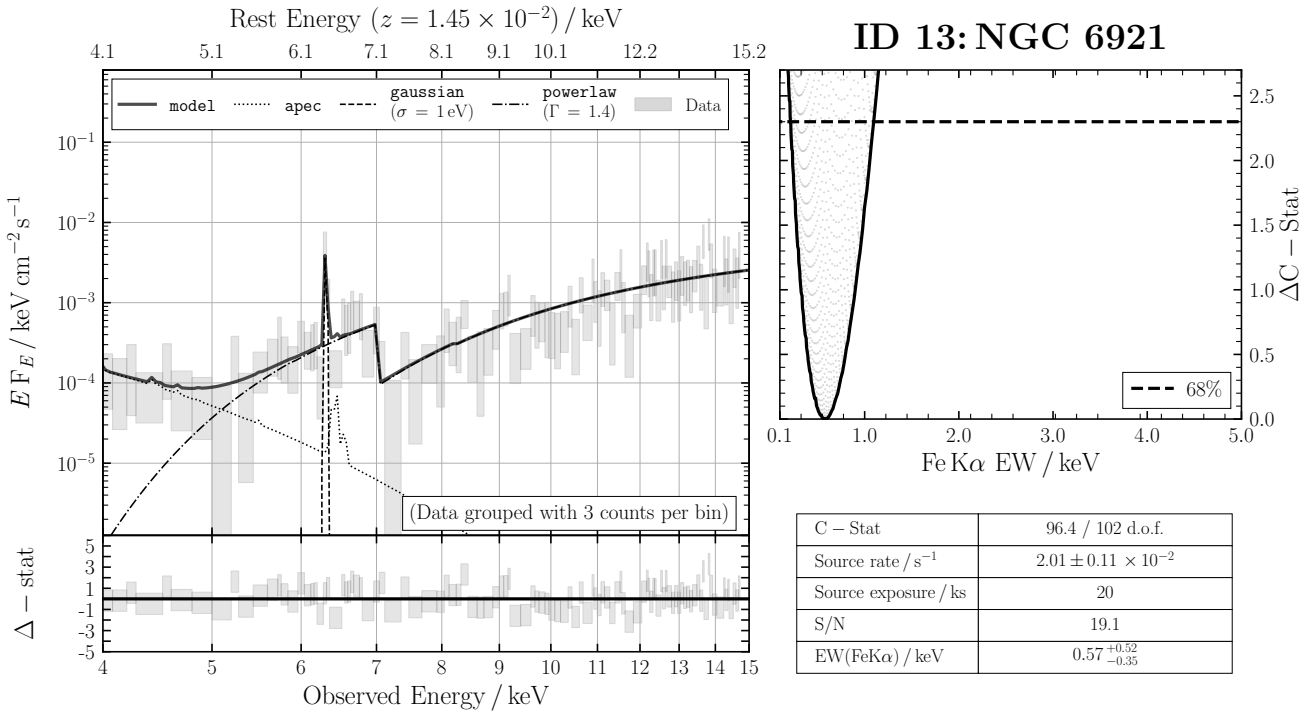

C − Stat	96.4 / 102 d.o.f.
Source rate / s^{-1}	$2.01 \pm 0.11 \times 10^{-2}$
Source exposure / ks	20
S/N	19.1
EW(FeKα) / keV	$0.57^{+0.52}_{-0.35}$

Figure B12. ID 13: NGC 6921

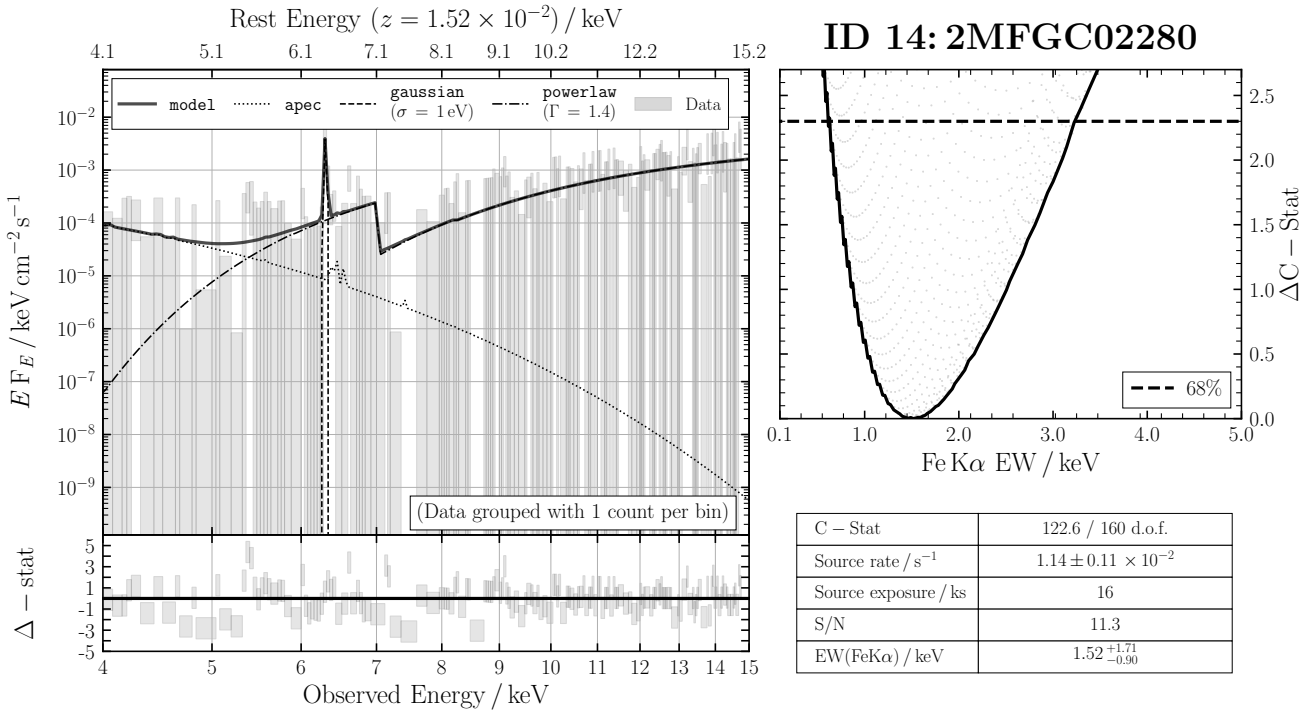

C − Stat	122.6 / 160 d.o.f.
Source rate / s^{-1}	$1.14 \pm 0.11 \times 10^{-2}$
Source exposure / ks	16
S/N	11.3
EW(FeKα) / keV	$1.52^{+1.71}_{-0.90}$

Figure B13. ID 14: 2MFGC02280

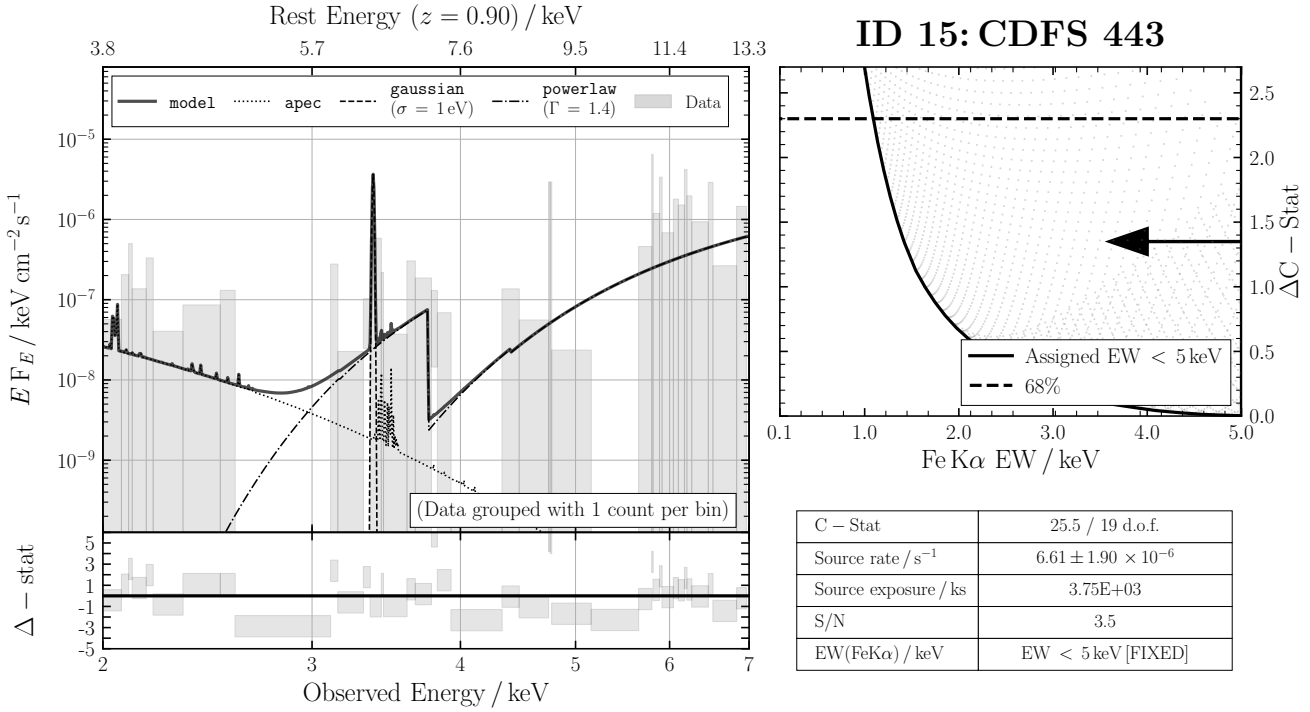

C − Stat	25.5 / 19 d.o.f.
Source rate / s^{-1}	$6.61 \pm 1.90 \times 10^{-6}$
Source exposure / ks	3.75E+03
S/N	3.5
EW(FeKα) / keV	EW < 5 keV [FIXED]

Figure B14. ID 15: CDFS 443

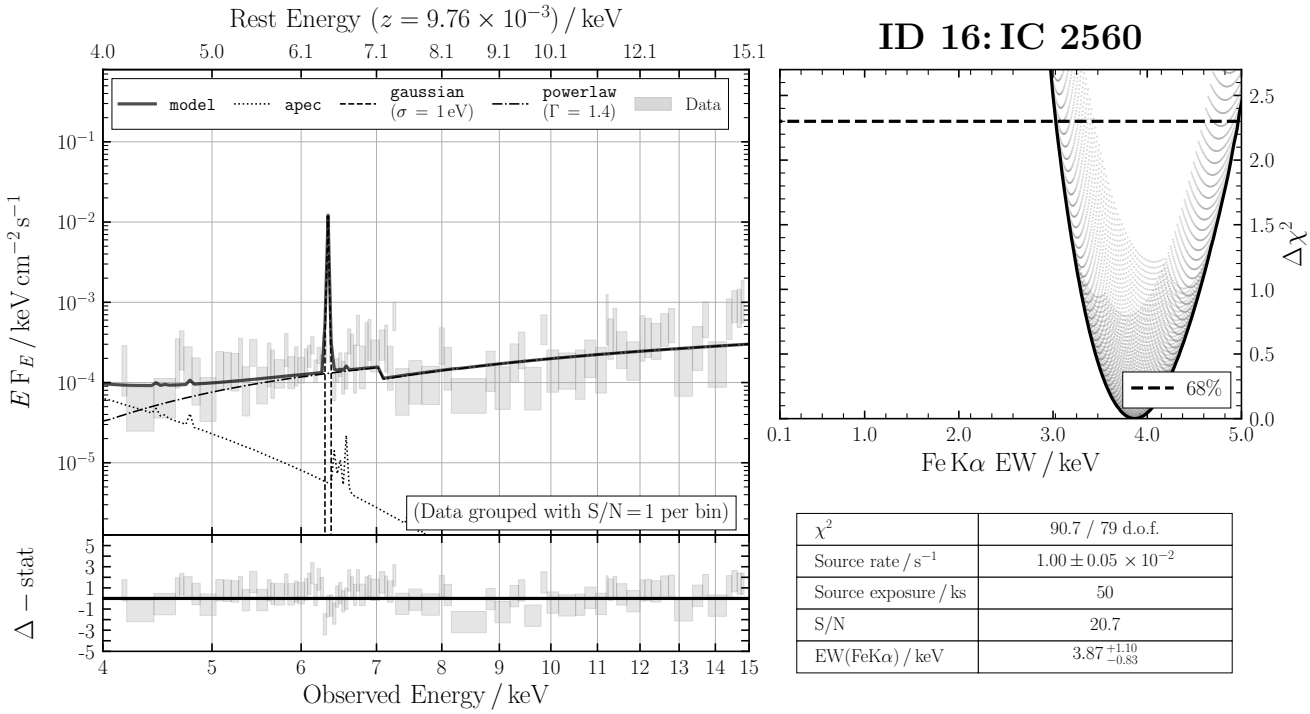

χ^2	90.7 / 79 d.o.f.
Source rate / s^{-1}	$1.00 \pm 0.05 \times 10^{-2}$
Source exposure / ks	50
S/N	20.7
EW(FeKα) / keV	$3.87^{+1.10}_{-0.83}$

Figure B15. ID 16: IC 2560

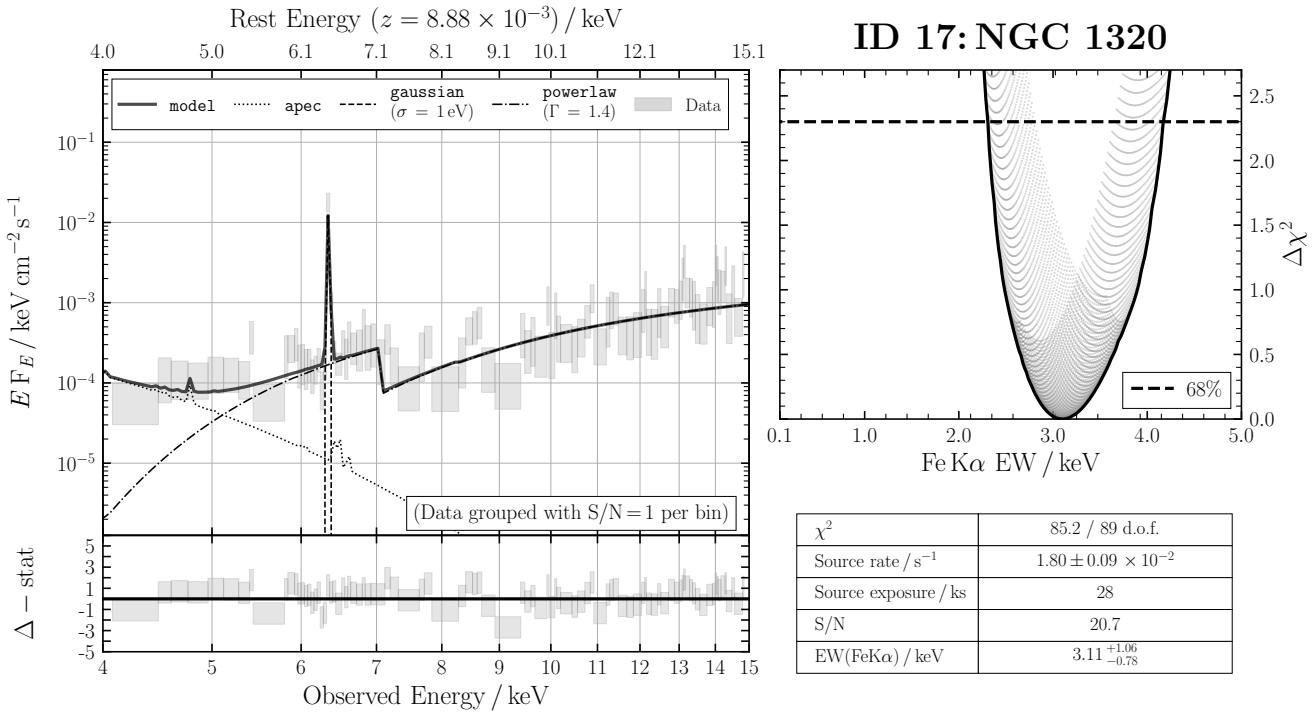

χ^2	85.2 / 89 d.o.f.
Source rate / s^{-1}	$1.80 \pm 0.09 \times 10^{-2}$
Source exposure / ks	28
S/N	20.7
EW(FeKα) / keV	$3.11^{+1.06}_{-0.78}$

Figure B16. ID 17: NGC 1320

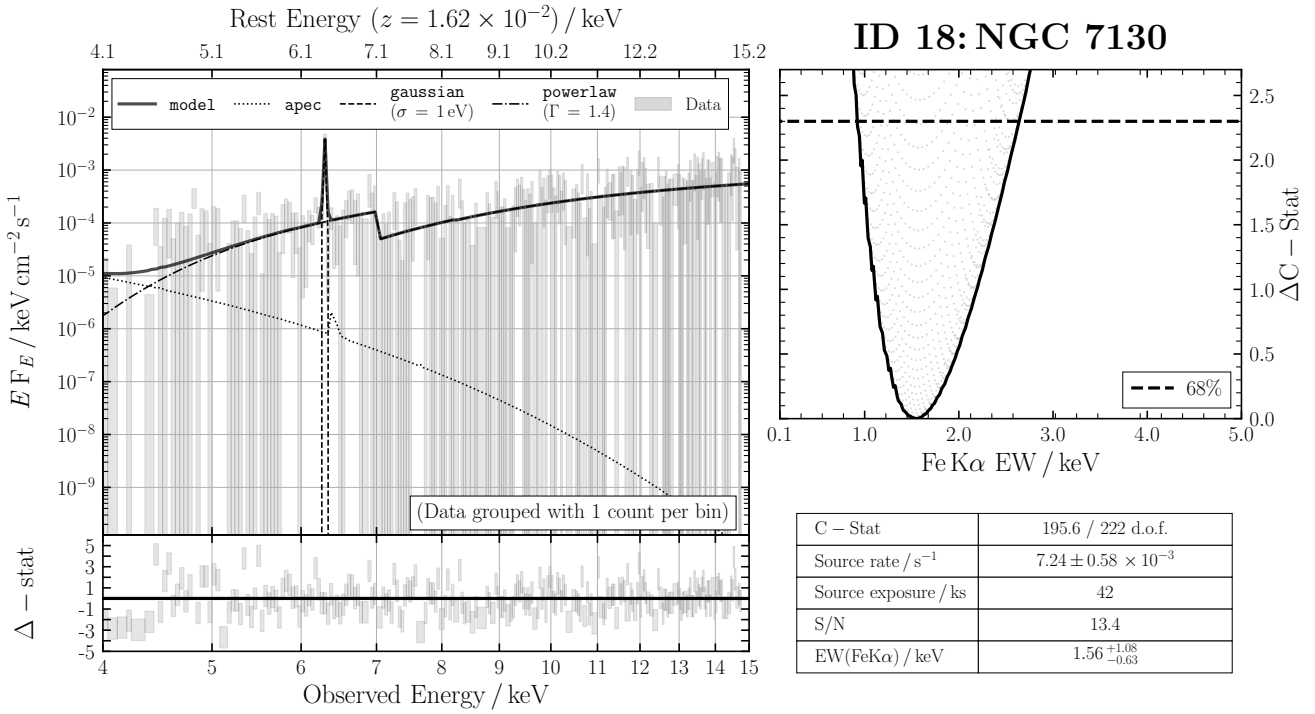

C − Stat	195.6 / 222 d.o.f.
Source rate / s^{-1}	$7.24 \pm 0.58 \times 10^{-3}$
Source exposure / ks	42
S/N	13.4
EW(FeKα) / keV	$1.56^{+1.08}_{-0.63}$

Figure B17. ID 18: NGC 7130

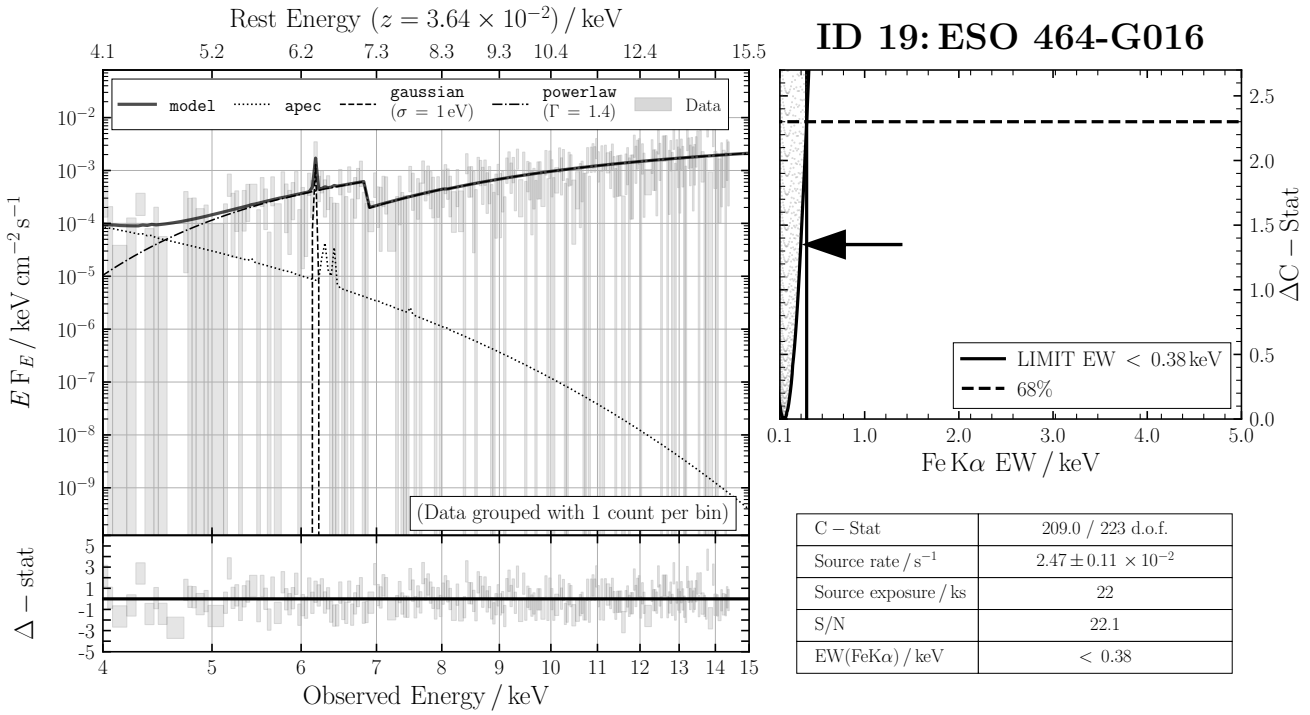

C − Stat	209.0 / 223 d.o.f.
Source rate / s^{-1}	$2.47 \pm 0.11 \times 10^{-2}$
Source exposure / ks	22
S/N	22.1
EW(FeKα) / keV	< 0.38

Figure B18. ID 19: ESO 464-G016

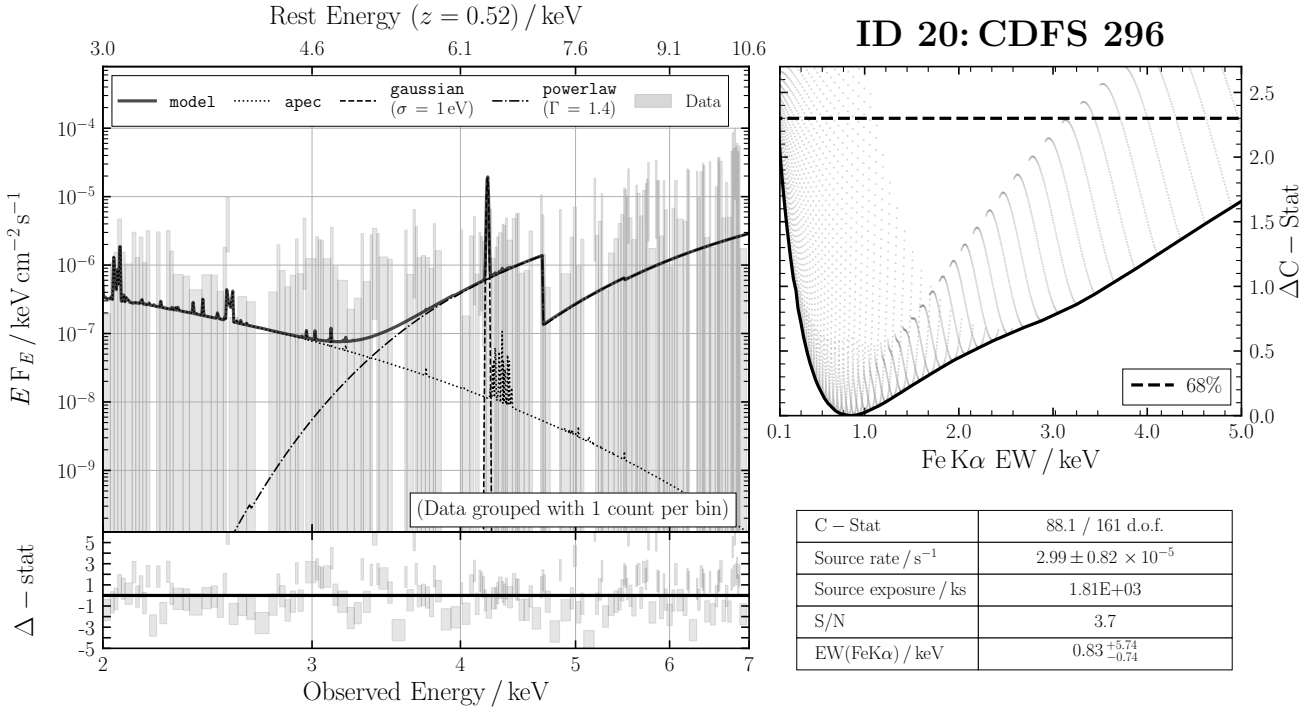

C − Stat	88.1 / 161 d.o.f.
Source rate / s^{-1}	$2.99 \pm 0.82 \times 10^{-5}$
Source exposure / ks	1.81E+03
S/N	3.7
EW(FeKα) / keV	$0.83^{+5.74}_{-0.74}$

Figure B19. ID 20: CDFS 296

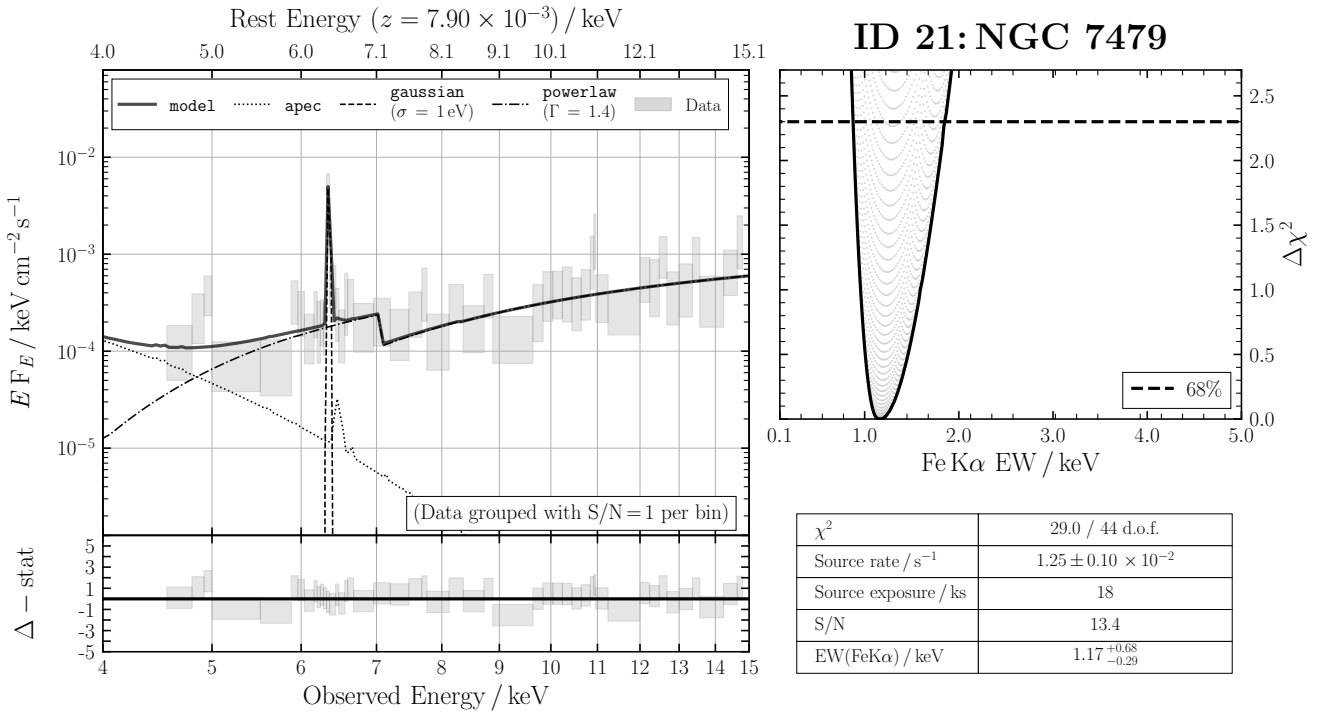

χ^2	29.0 / 44 d.o.f.
Source rate / s^{-1}	$1.25 \pm 0.10 \times 10^{-2}$
Source exposure / ks	18
S/N	13.4
EW(FeKα) / keV	$1.17^{+0.68}_{-0.29}$

Figure B20. ID 21: NGC 7479

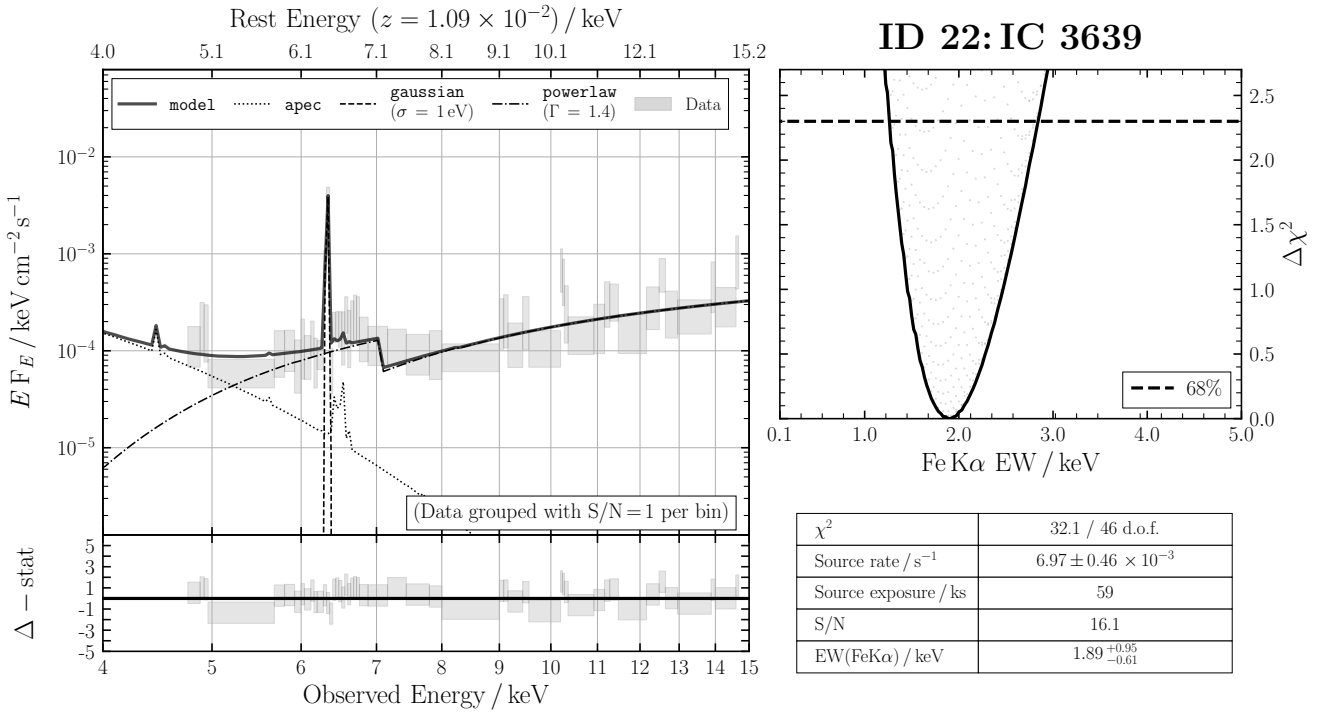

χ^2	32.1 / 46 d.o.f.
Source rate / s^{-1}	$6.97 \pm 0.46 \times 10^{-3}$
Source exposure / ks	59
S/N	16.1
EW(FeKα) / keV	$1.89^{+0.95}_{-0.61}$

Figure B21. ID 22: IC 3639

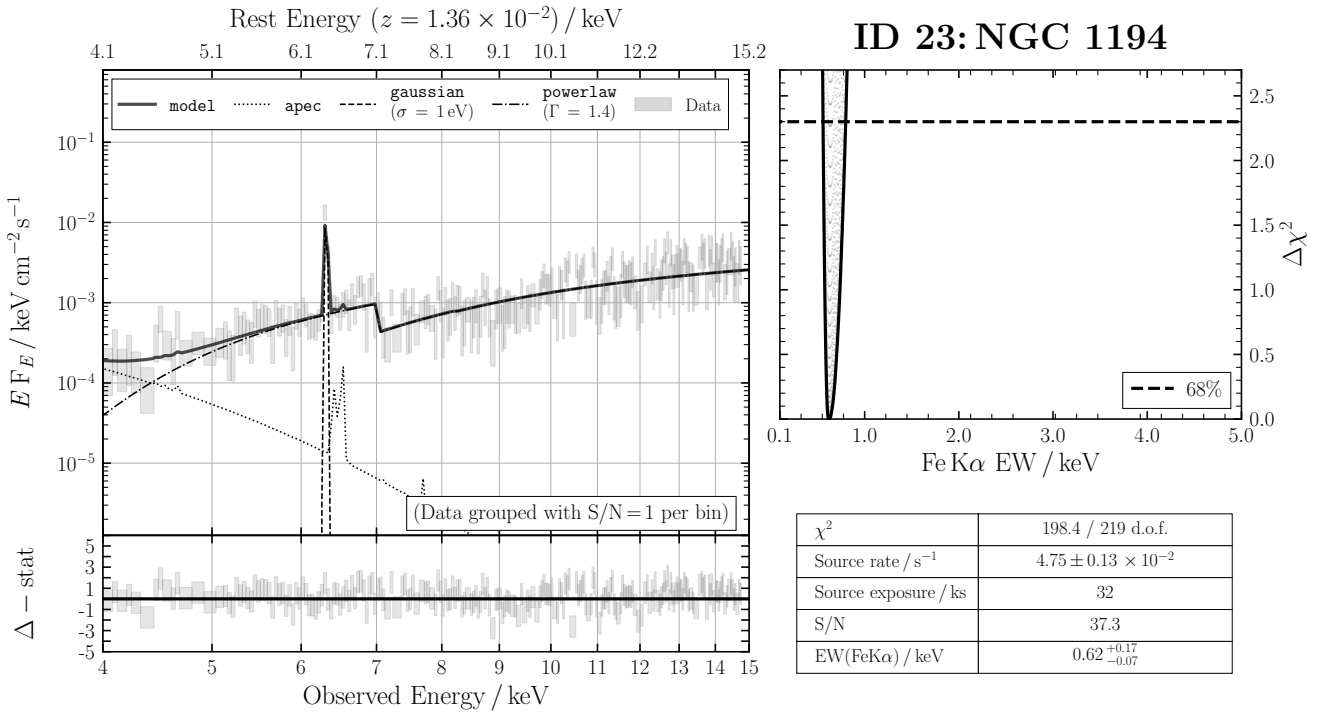

χ^2	198.4 / 219 d.o.f.
Source rate / s^{-1}	$4.75 \pm 0.13 \times 10^{-2}$
Source exposure / ks	32
S/N	37.3
EW(FeKα) / keV	$0.62^{+0.17}_{-0.07}$

Figure B22. ID 23: NGC 1194

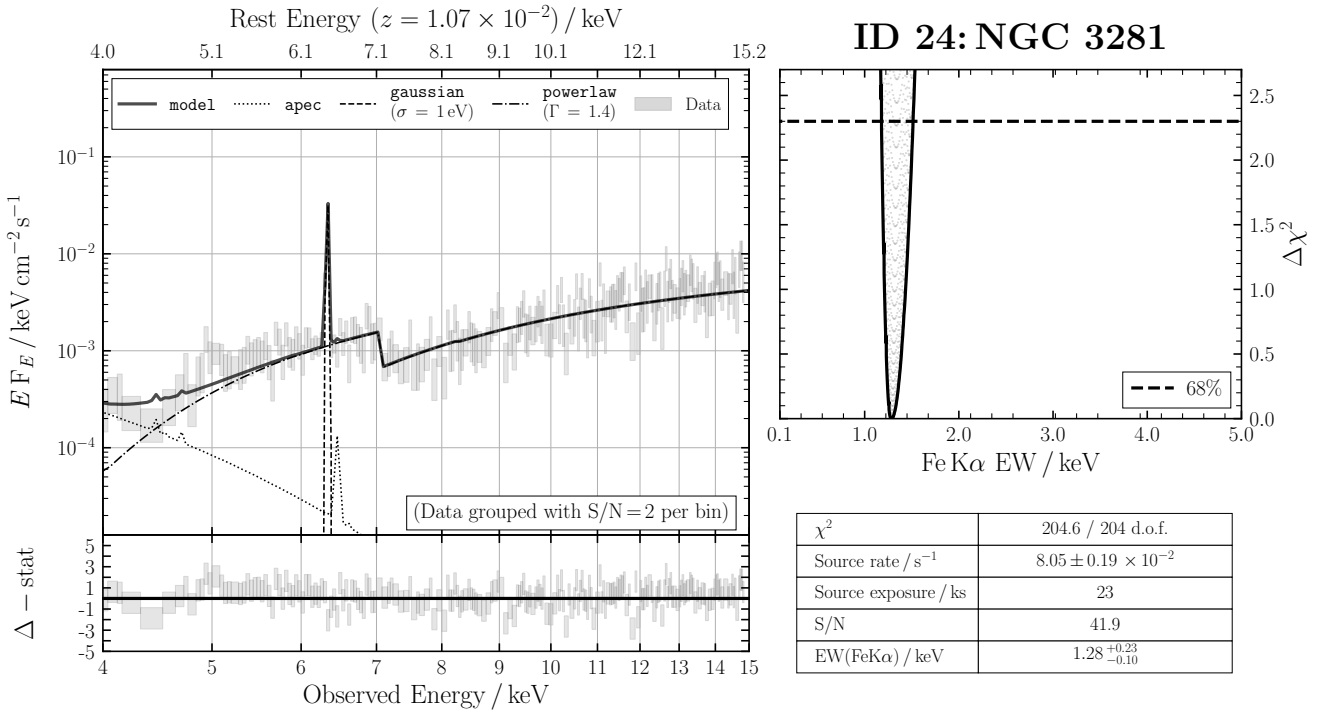

χ^2	204.6 / 204 d.o.f.
Source rate / s^{-1}	$8.05 \pm 0.19 \times 10^{-2}$
Source exposure / ks	23
S/N	41.9
EW(FeKα) / keV	$1.28^{+0.23}_{-0.10}$

Figure B23. ID 24: NGC 3281

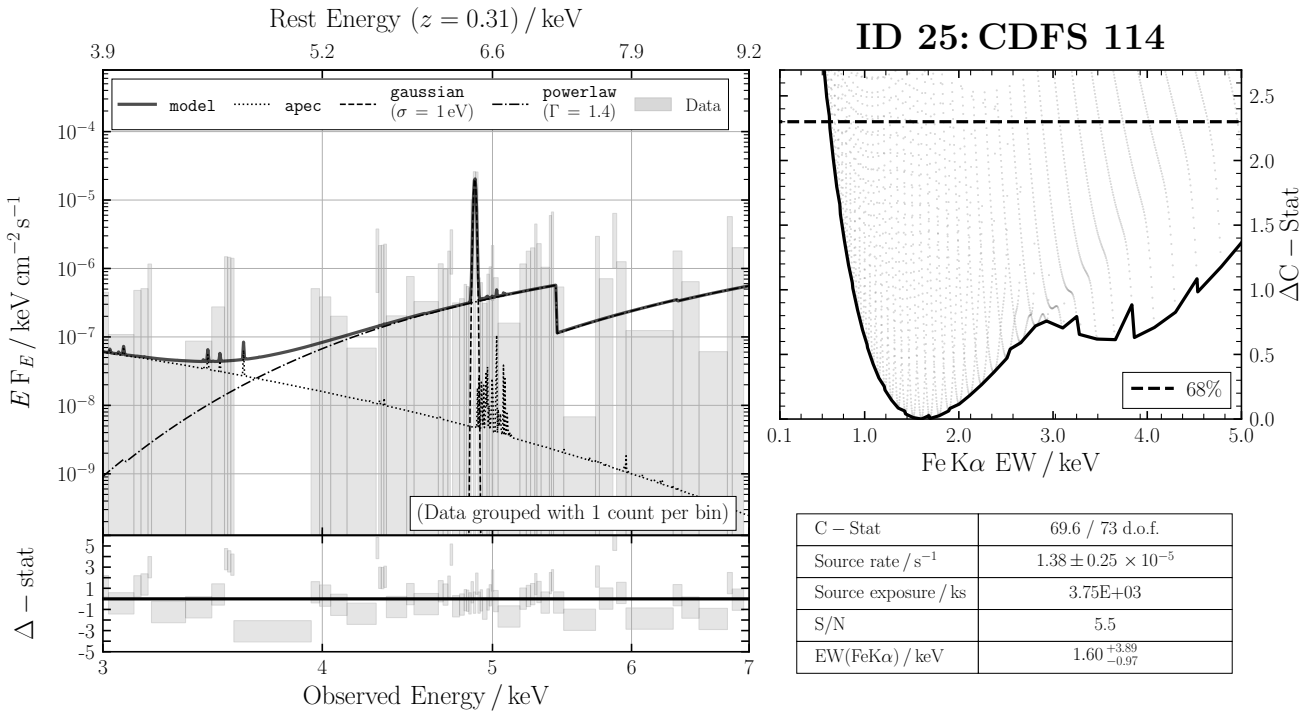

C − Stat	69.6 / 73 d.o.f.
Source rate / s^{-1}	$1.38 \pm 0.25 \times 10^{-5}$
Source exposure / ks	3.75E+03
S/N	5.5
EW(FeKα) / keV	$1.60^{+3.89}_{-0.97}$

Figure B24. ID 25: CDFS 114

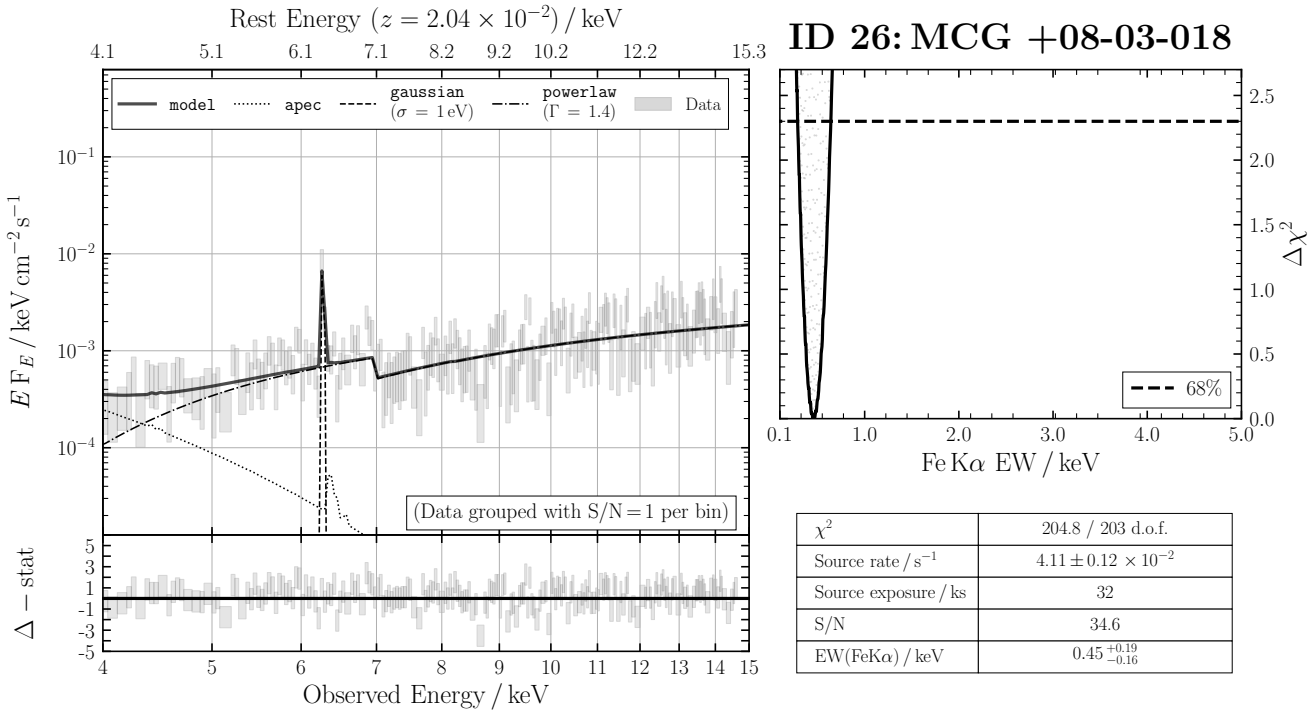

χ^2	204.8 / 203 d.o.f.
Source rate / s^{-1}	$4.11 \pm 0.12 \times 10^{-2}$
Source exposure / ks	32
S/N	34.6
EW(FeKα) / keV	$0.45^{+0.19}_{-0.16}$

Figure B25. ID 26: MCG +08-03-018

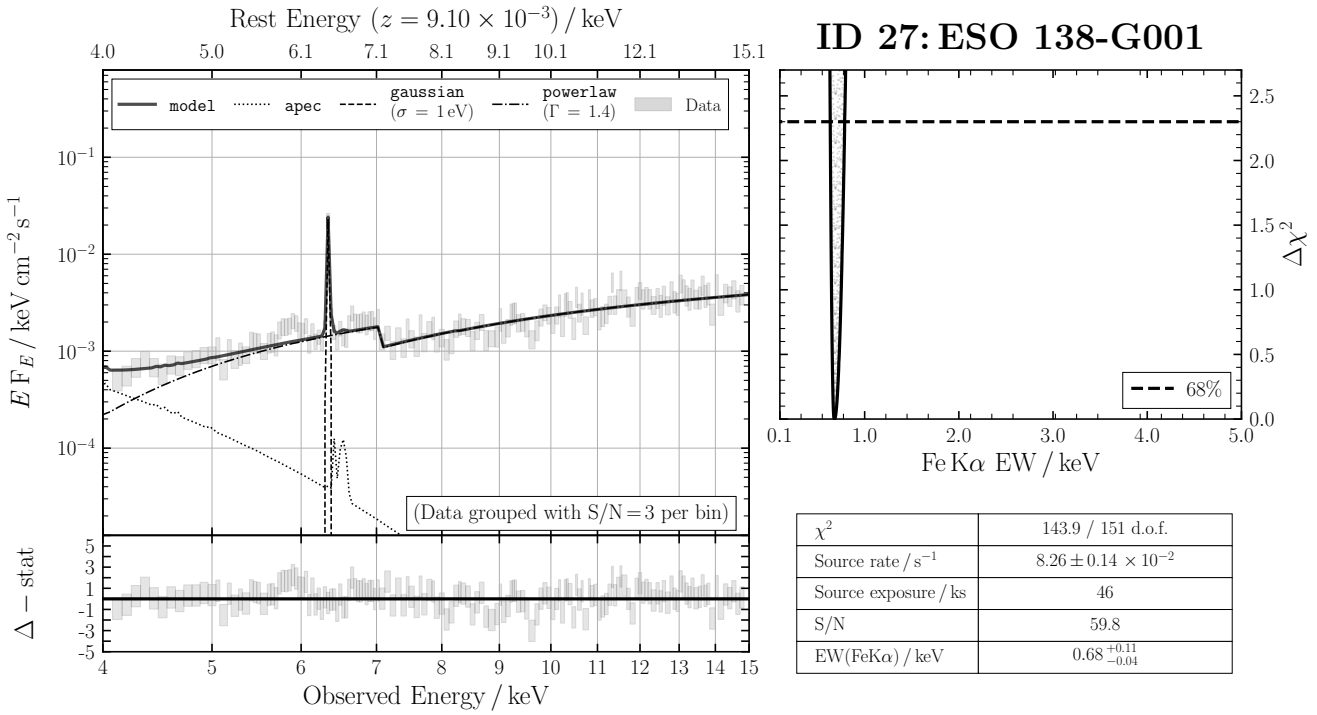

χ^2	143.9 / 151 d.o.f.
Source rate / s^{-1}	$8.26 \pm 0.14 \times 10^{-2}$
Source exposure / ks	46
S/N	59.8
EW(FeKα) / keV	$0.68^{+0.11}_{-0.04}$

Figure B26. ID 27: ESO 138-G001

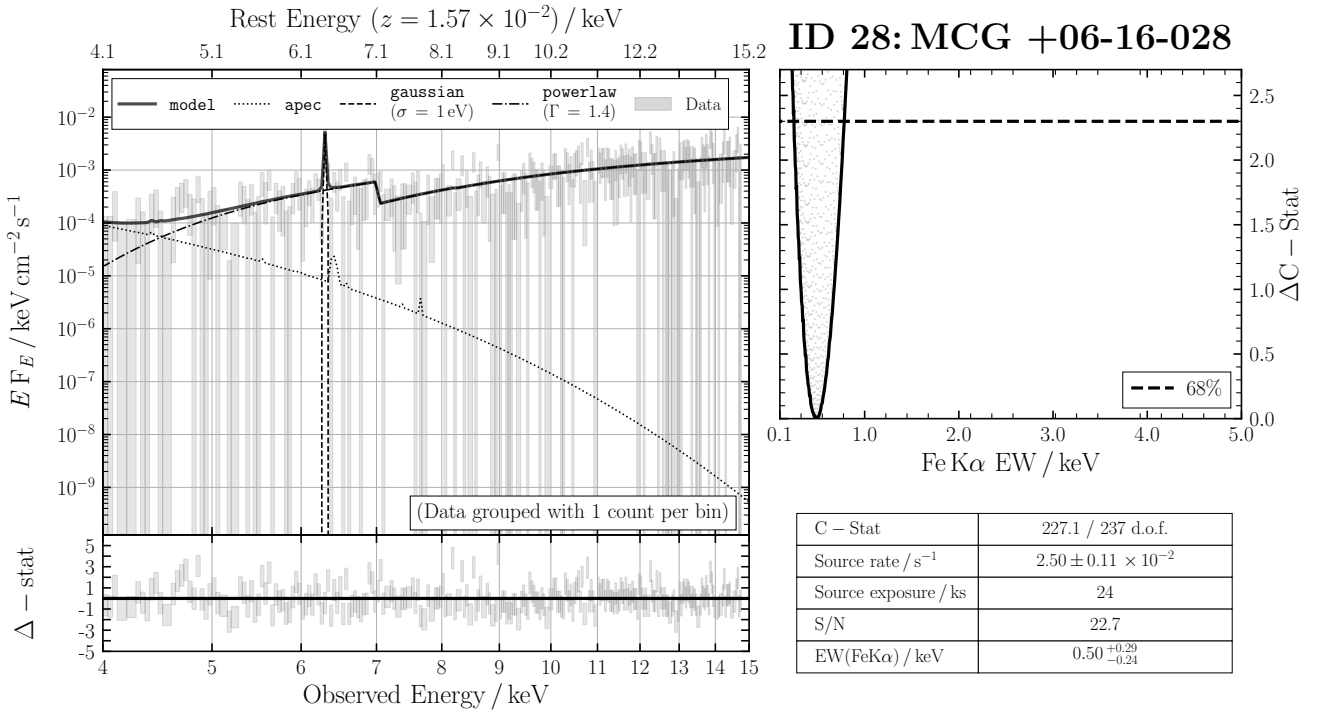

C − Stat	227.1 / 237 d.o.f.
Source rate / s^{-1}	$2.50 \pm 0.11 \times 10^{-2}$
Source exposure / ks	24
S/N	22.7
EW(FeKα) / keV	$0.50^{+0.29}_{-0.24}$

Figure B27. ID 28: MCG +06-16-028

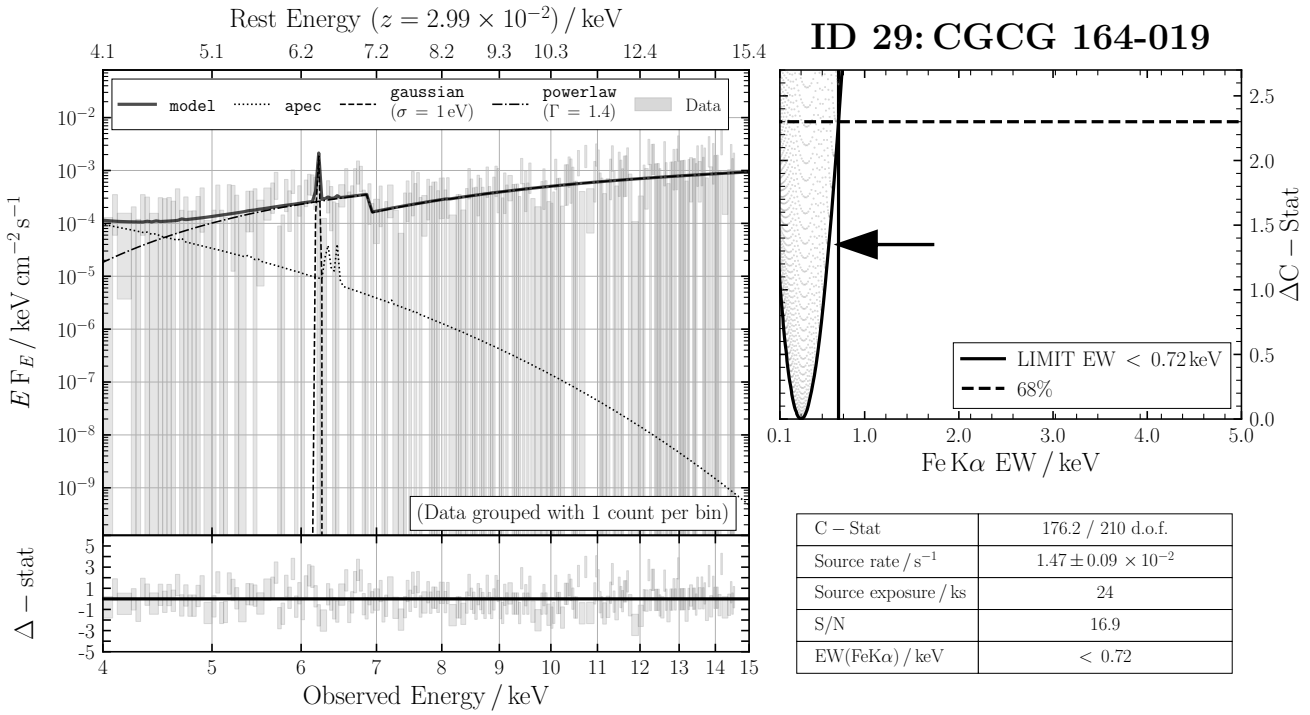

C − Stat	176.2 / 210 d.o.f.
Source rate / s^{-1}	$1.47 \pm 0.09 \times 10^{-2}$
Source exposure / ks	24
S/N	16.9
EW(FeKα) / keV	< 0.72

Figure B28. ID 29: CGCG 164-019

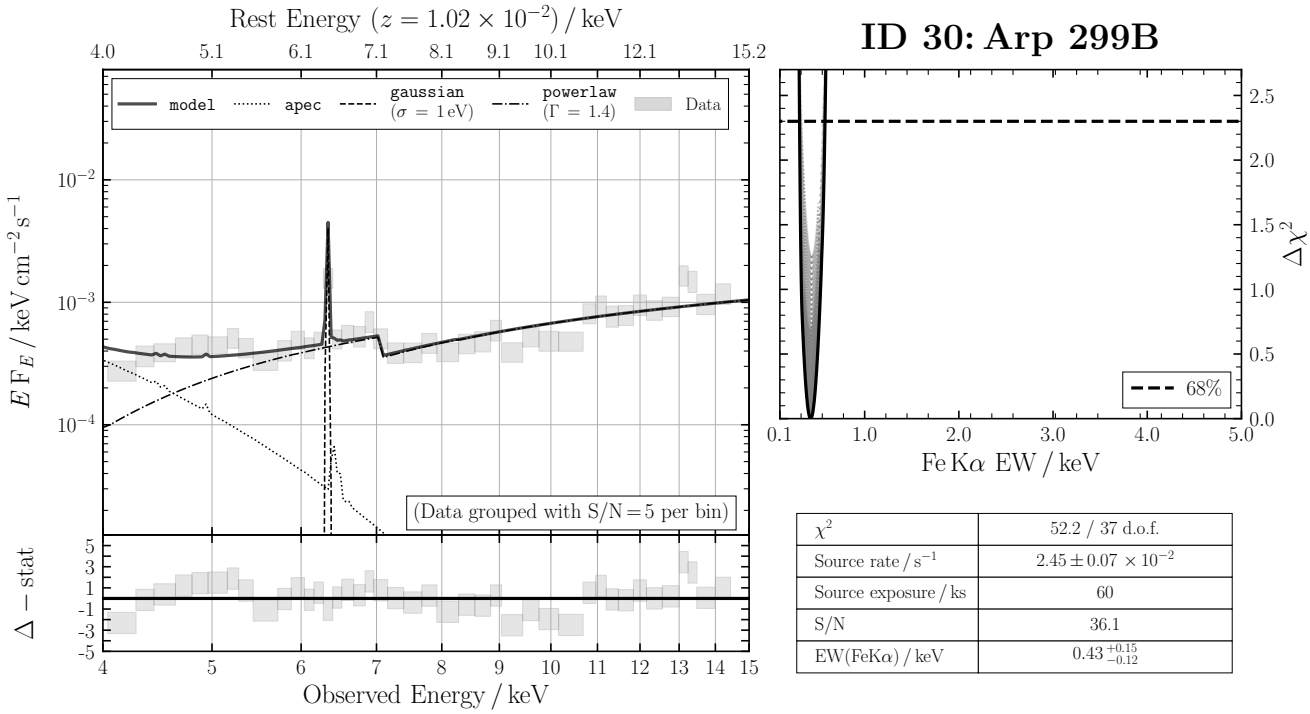

χ^2	52.2 / 37 d.o.f.
Source rate / s^{-1}	$2.45 \pm 0.07 \times 10^{-2}$
Source exposure / ks	60
S/N	36.1
EW(FeKα) / keV	$0.43^{+0.15}_{-0.12}$

Figure B29. ID 30: Arp 299B

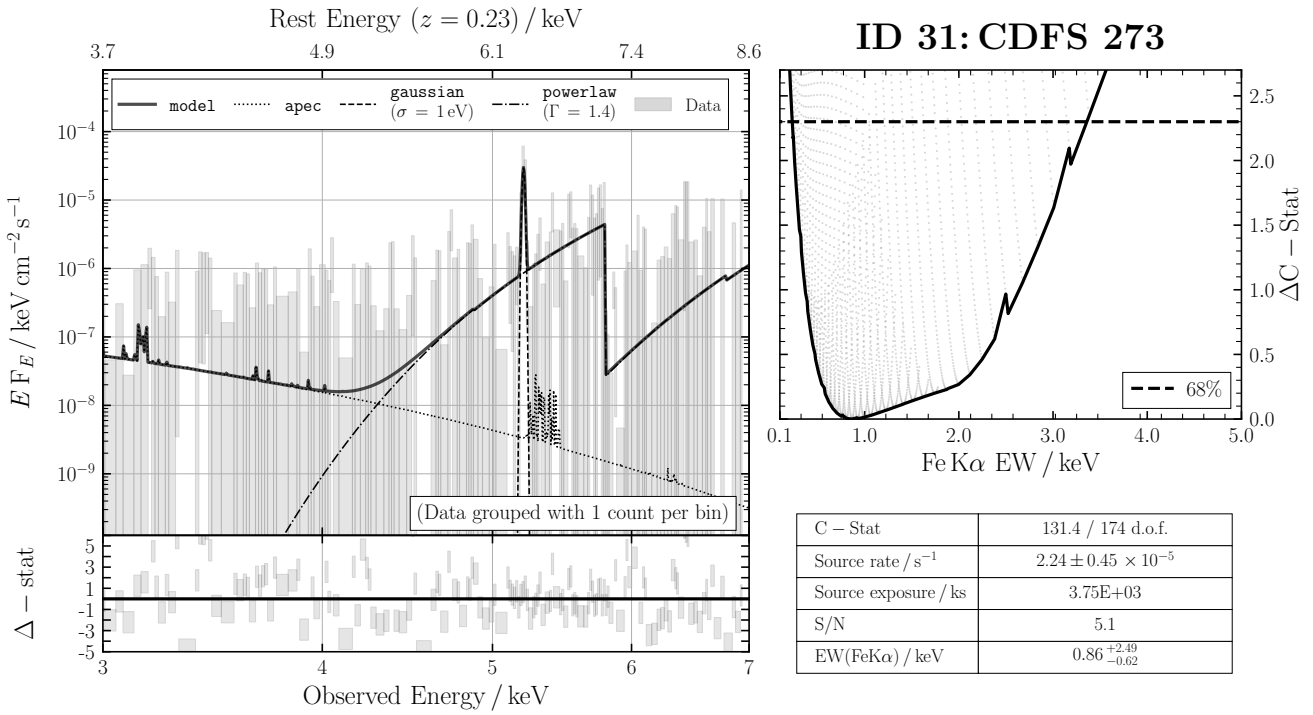

C − Stat	131.4 / 174 d.o.f.
Source rate / s^{-1}	$2.24 \pm 0.45 \times 10^{-5}$
Source exposure / ks	3.75E+03
S/N	5.1
EW(FeKα) / keV	$0.86^{+2.49}_{-0.62}$

Figure B30. ID 31: CDFS 273

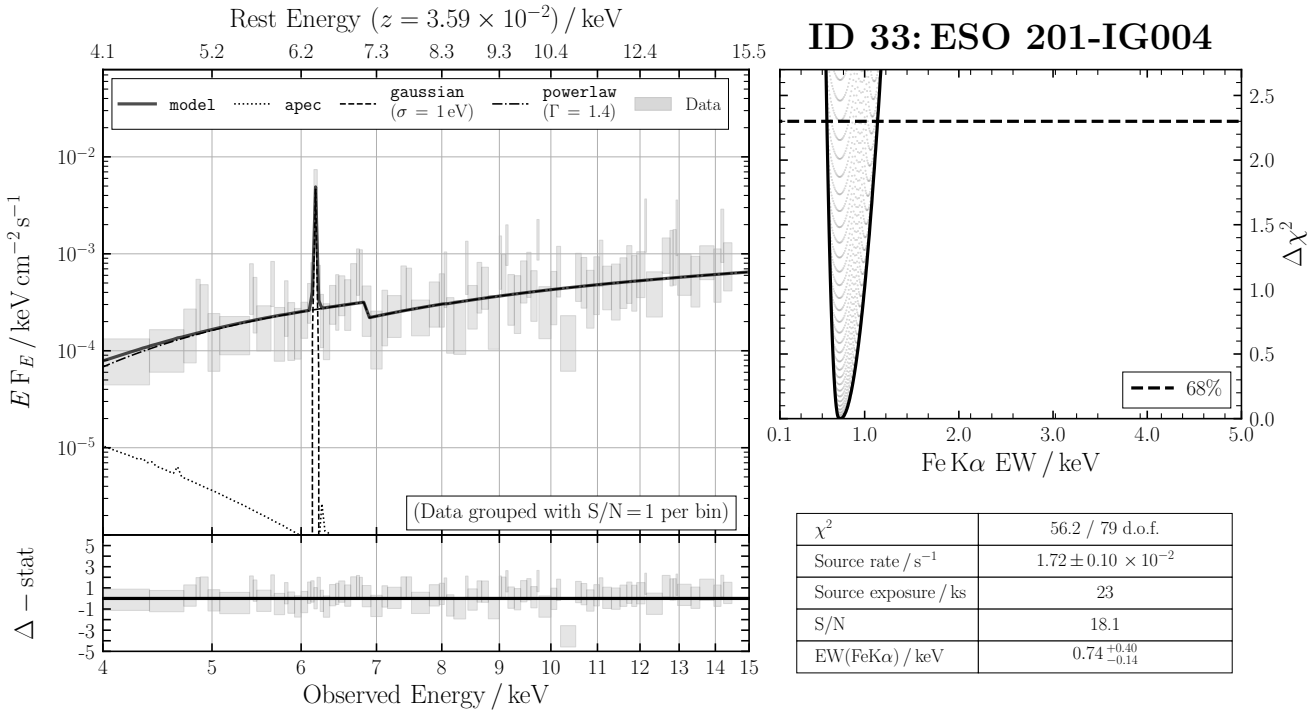

χ^2	56.2 / 79 d.o.f.
Source rate / s^{-1}	$1.72 \pm 0.10 \times 10^{-2}$
Source exposure / ks	23
S/N	18.1
EW(FeKα) / keV	$0.74^{+0.40}_{-0.14}$

Figure B31. ID 33: ESO 201-IG004

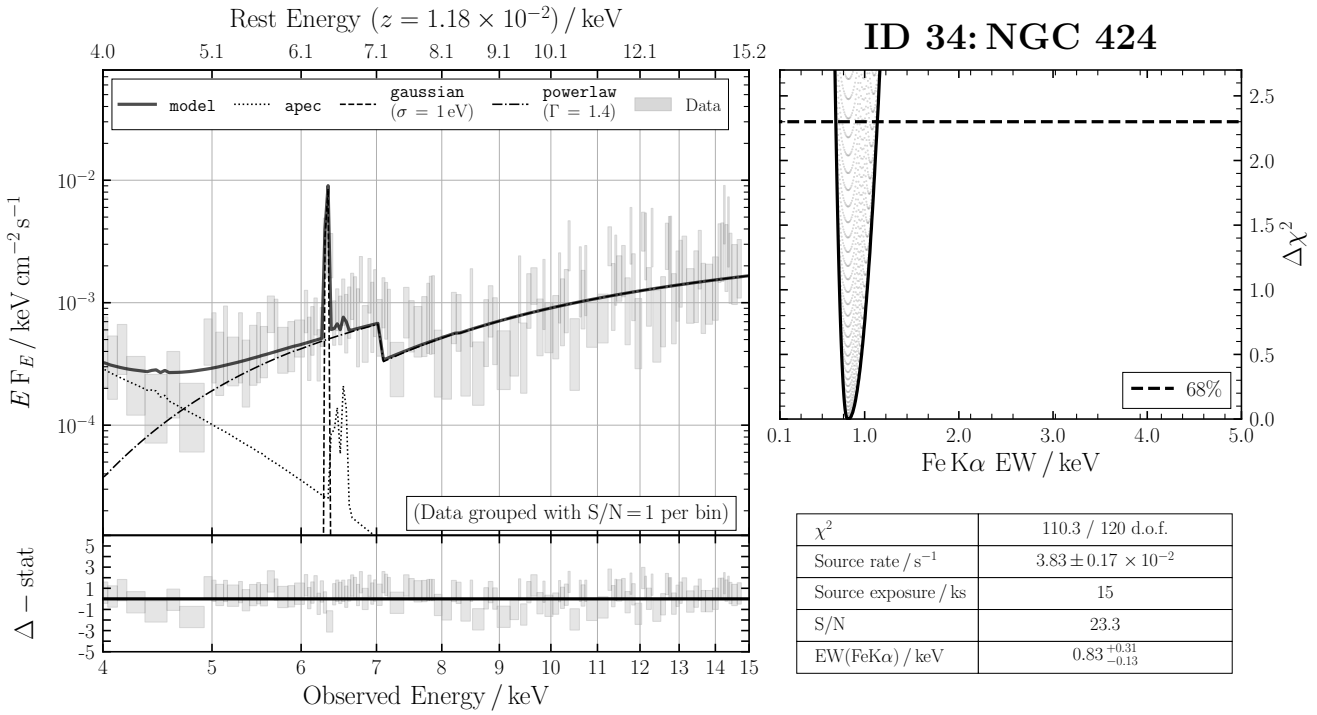

χ^2	110.3 / 120 d.o.f.
Source rate / s^{-1}	$3.83 \pm 0.17 \times 10^{-2}$
Source exposure / ks	15
S/N	23.3
EW(FeKα) / keV	$0.83^{+0.31}_{-0.13}$

Figure B32. ID 34: NGC 424

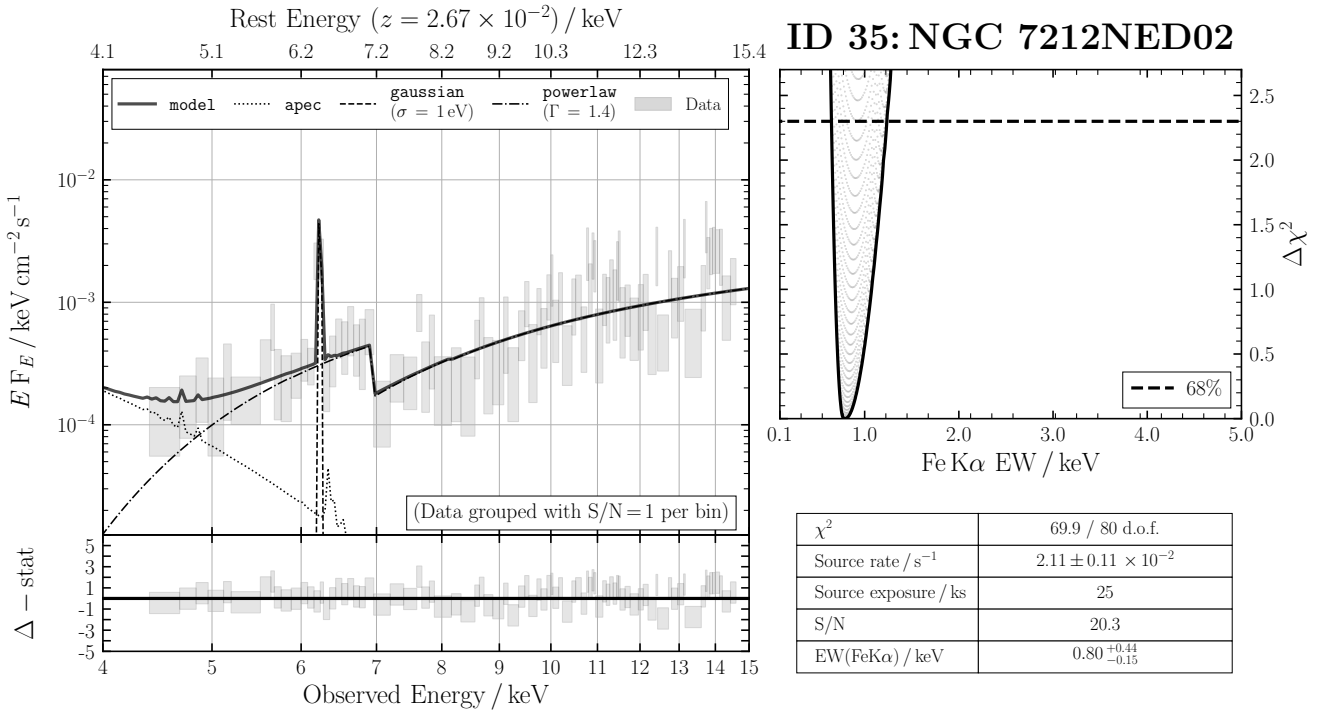

χ^2	69.9 / 80 d.o.f.
Source rate / s^{-1}	$2.11 \pm 0.11 \times 10^{-2}$
Source exposure / ks	25
S/N	20.3
EW(FeKα) / keV	$0.80^{+0.44}_{-0.15}$

Figure B33. ID 35: NGC 7212NED02

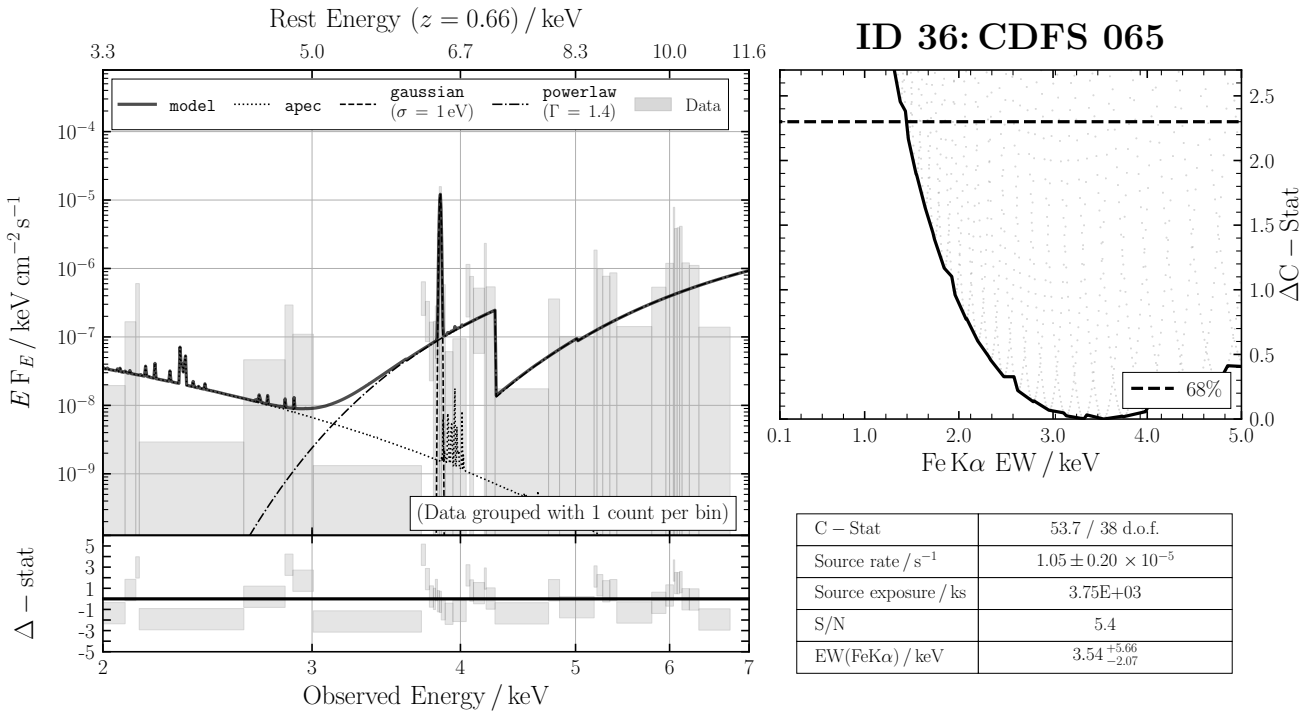

C − Stat	53.7 / 38 d.o.f.
Source rate / s^{-1}	$1.05 \pm 0.20 \times 10^{-5}$
Source exposure / ks	3.75E+03
S/N	5.4
EW(FeKα) / keV	$3.54^{+5.66}_{-2.07}$

Figure B34. ID 36: CDFS 065

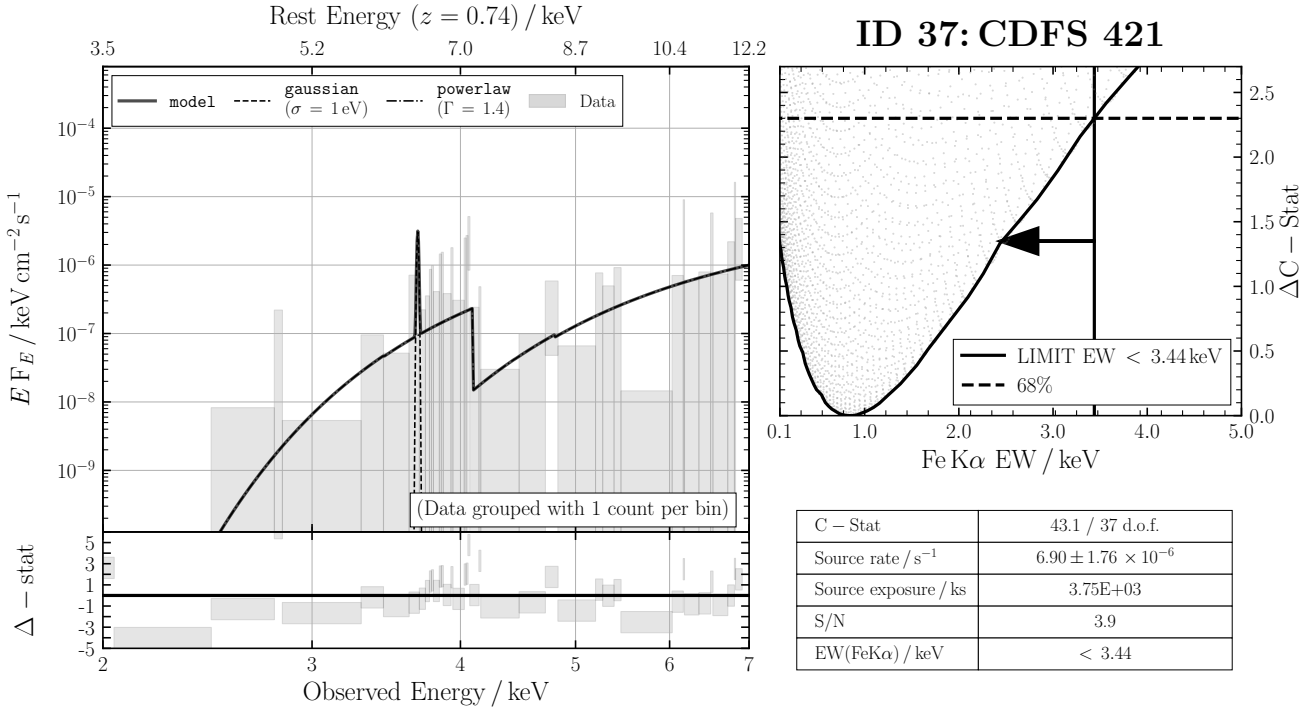

C − Stat	43.1 / 37 d.o.f.
Source rate / s^{-1}	$6.90 \pm 1.76 \times 10^{-6}$
Source exposure / ks	3.75E+03
S/N	3.9
EW(FeKα) / keV	< 3.44

Figure B35. ID 37: CDFS 421

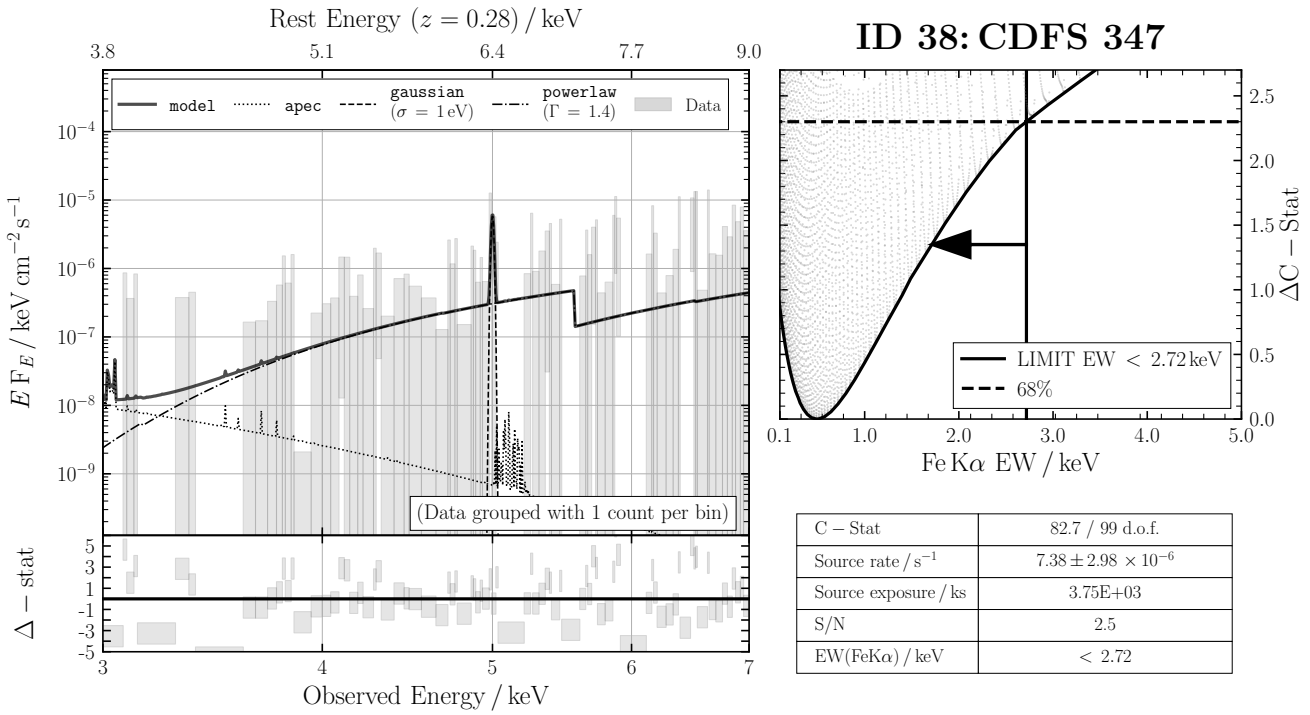

C − Stat	82.7 / 99 d.o.f.
Source rate / s^{-1}	$7.38 \pm 2.98 \times 10^{-6}$
Source exposure / ks	3.75E+03
S/N	2.5
EW(FeKα) / keV	< 2.72

Figure B36. ID 38: CDFS 347

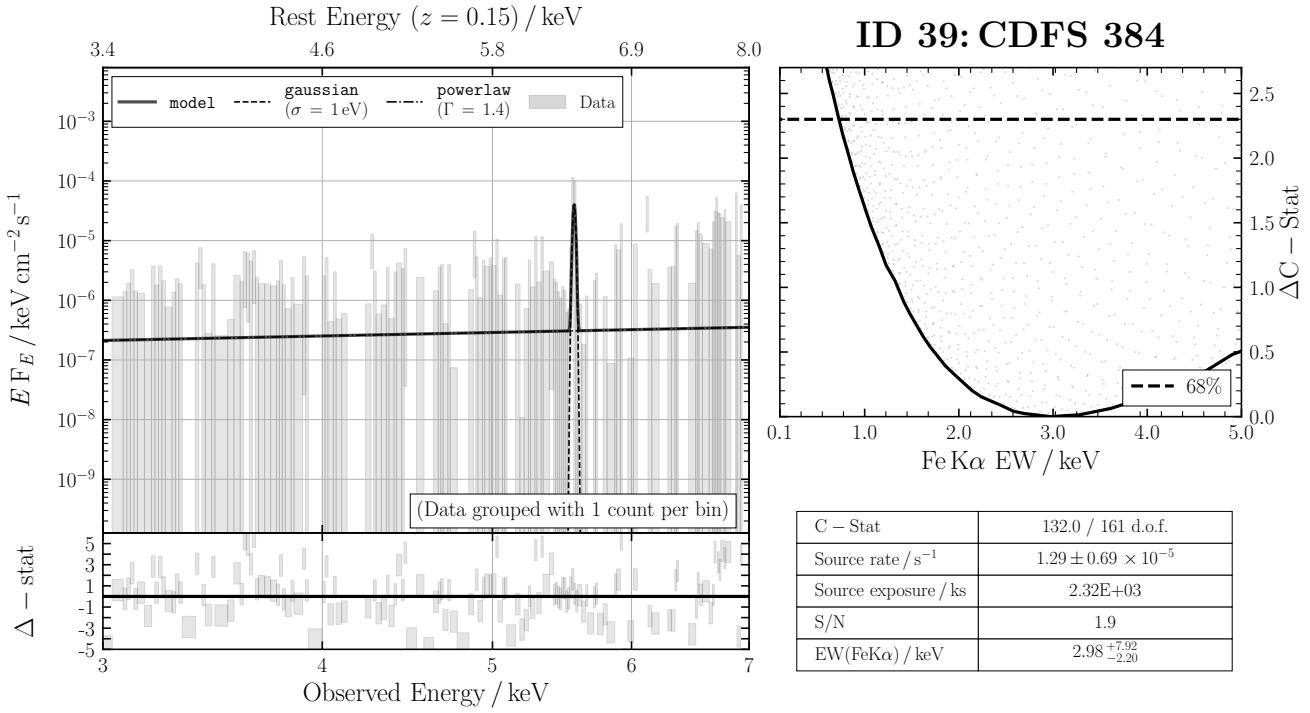

C − Stat	132.0 / 161 d.o.f.
Source rate / s^{-1}	$1.29 \pm 0.69 \times 10^{-5}$
Source exposure / ks	2.32E+03
S/N	1.9
EW(FeKα) / keV	$2.98^{+7.92}_{-2.20}$

Figure B37. ID 39: CDFS 384

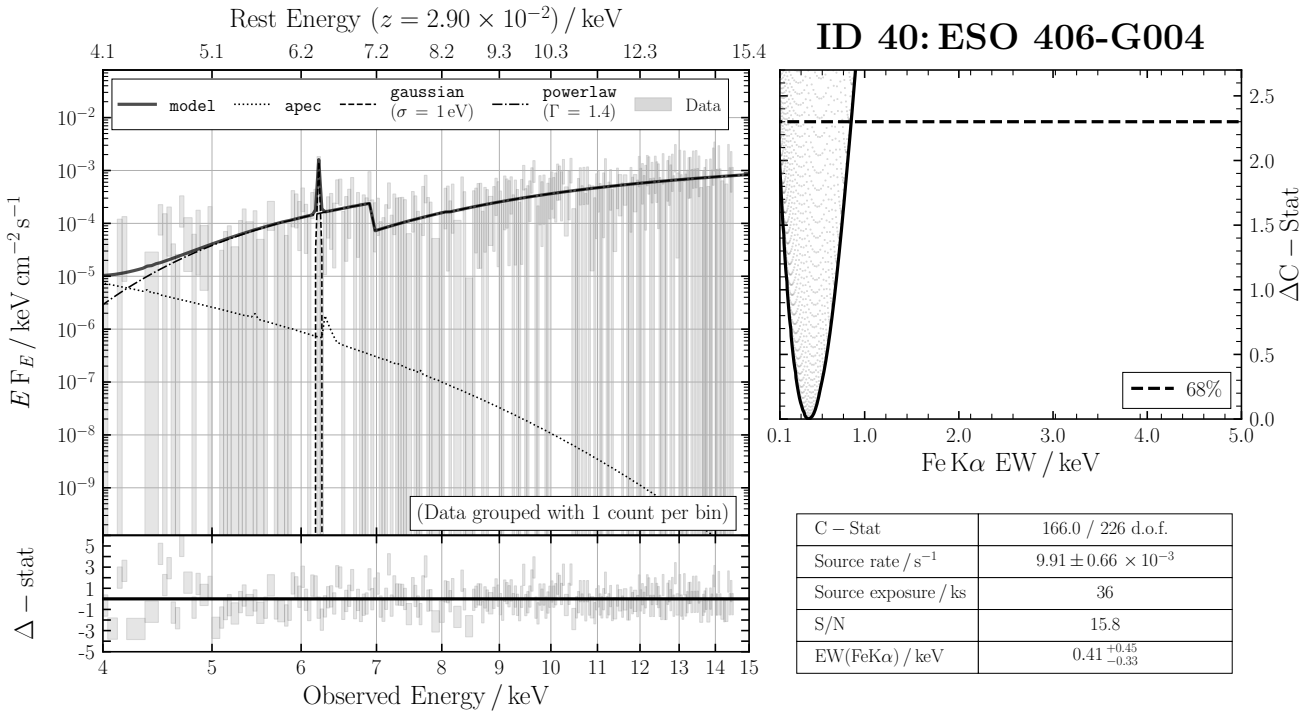

C − Stat	166.0 / 226 d.o.f.
Source rate / s^{-1}	$9.91 \pm 0.66 \times 10^{-3}$
Source exposure / ks	36
S/N	15.8
EW(FeKα) / keV	$0.41^{+0.45}_{-0.33}$

Figure B38. ID 40: ESO 406-G004

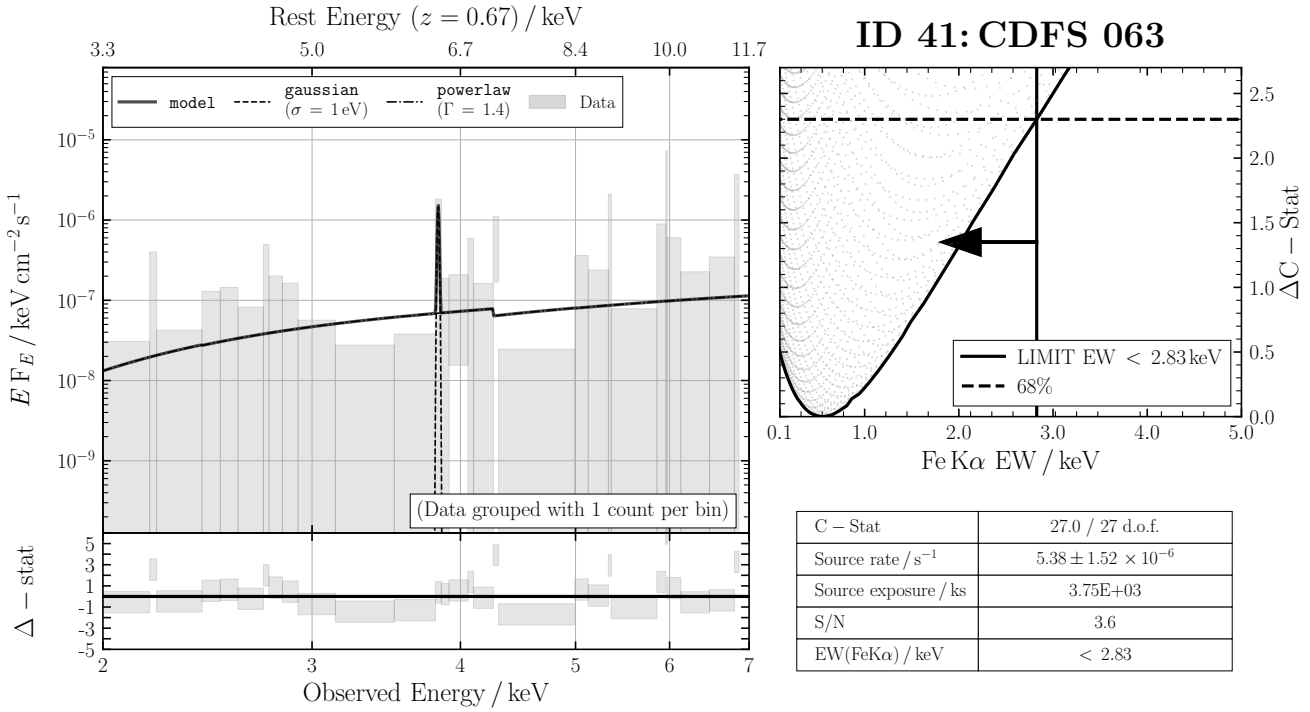

C − Stat	27.0 / 27 d.o.f.
Source rate / s^{-1}	$5.38 \pm 1.52 \times 10^{-6}$
Source exposure / ks	3.75E+03
S/N	3.6
EW(FeKα) / keV	< 2.83

Figure B39. ID 41: CDFS 063

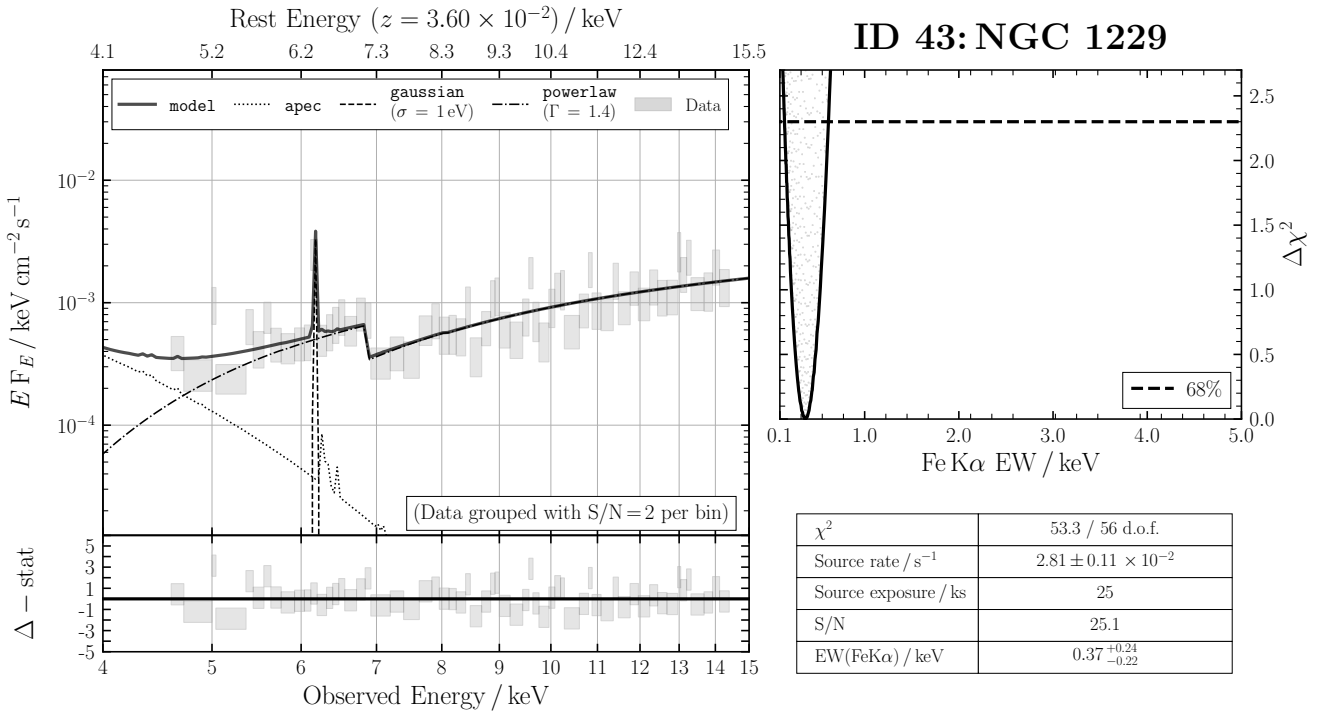

χ^2	53.3 / 56 d.o.f.
Source rate / s^{-1}	$2.81 \pm 0.11 \times 10^{-2}$
Source exposure / ks	25
S/N	25.1
EW(FeKα) / keV	$0.37^{+0.24}_{-0.22}$

Figure B40. ID 43: NGC 1229

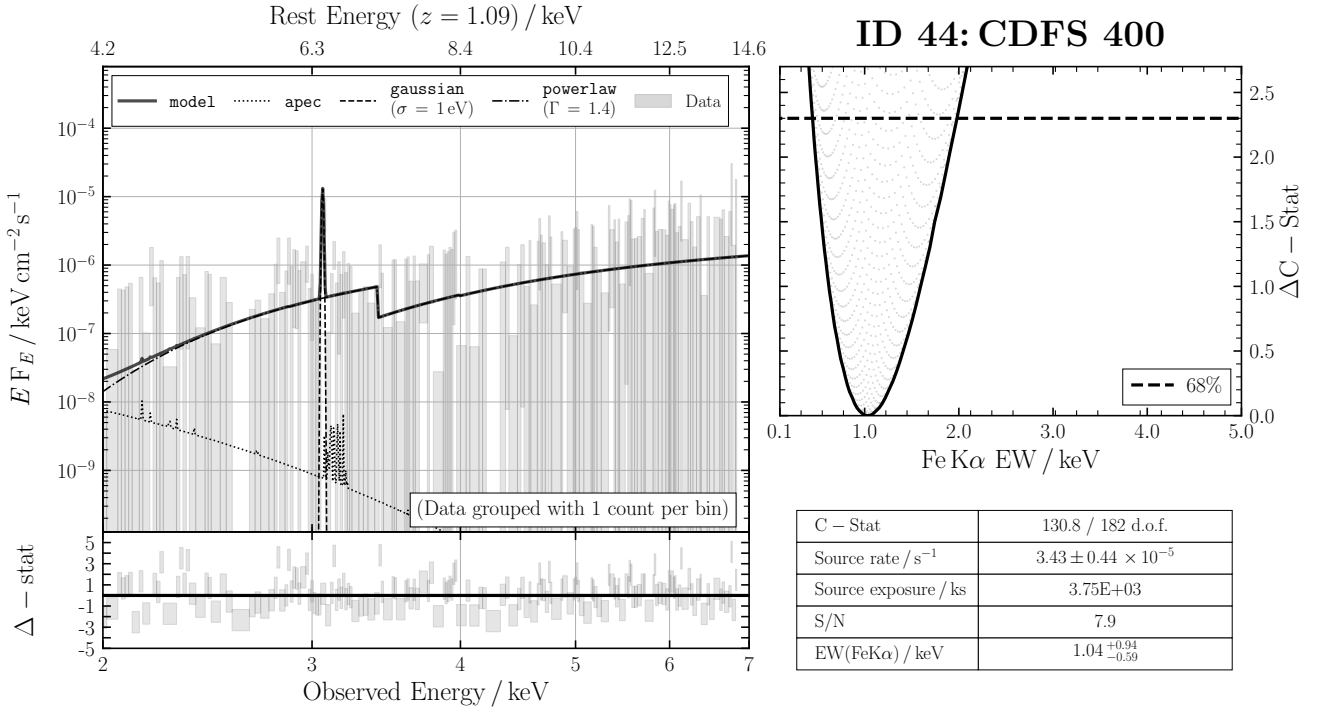

C − Stat	130.8 / 182 d.o.f.
Source rate / s^{-1}	$3.43 \pm 0.44 \times 10^{-5}$
Source exposure / ks	3.75E+03
S/N	7.9
EW(FeKα) / keV	$1.04^{+0.94}_{-0.59}$

Figure B41. ID 44: CDFS 400

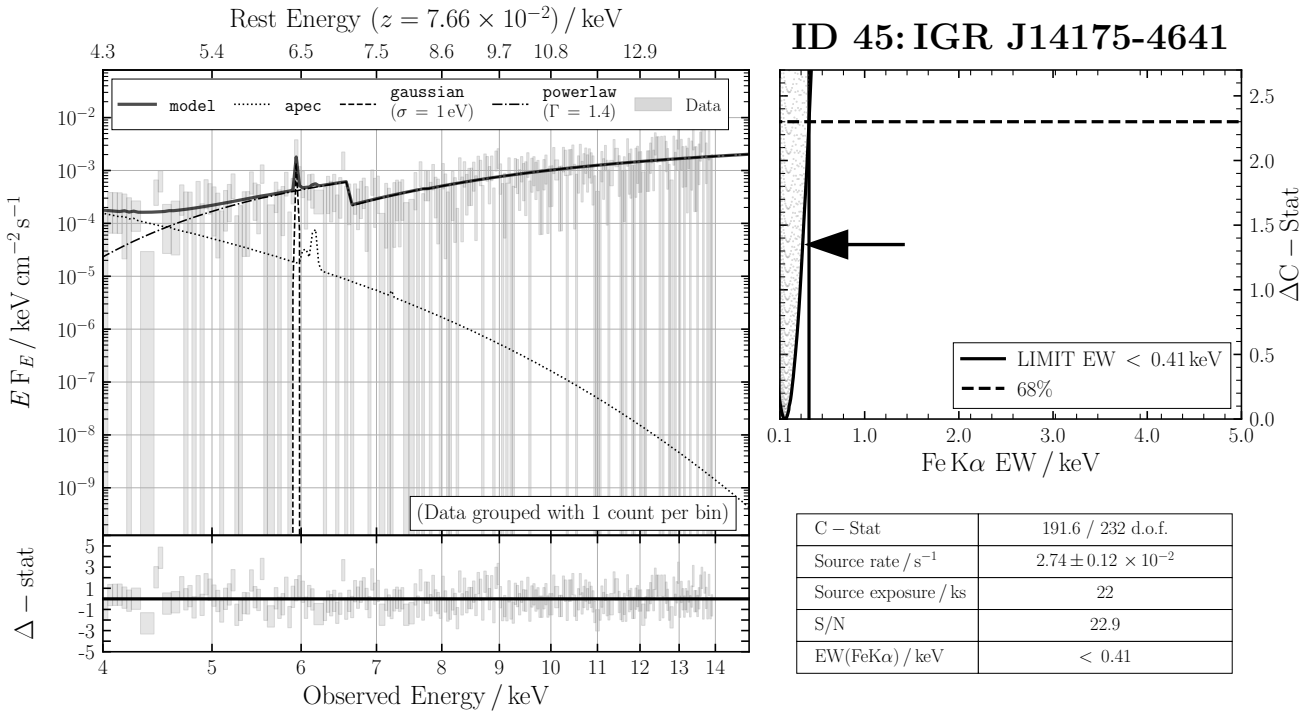

C − Stat	191.6 / 232 d.o.f.
Source rate / s^{-1}	$2.74 \pm 0.12 \times 10^{-2}$
Source exposure / ks	22
S/N	22.9
EW(FeKα) / keV	< 0.41

Figure B42. ID 45: IGR J14175-4641

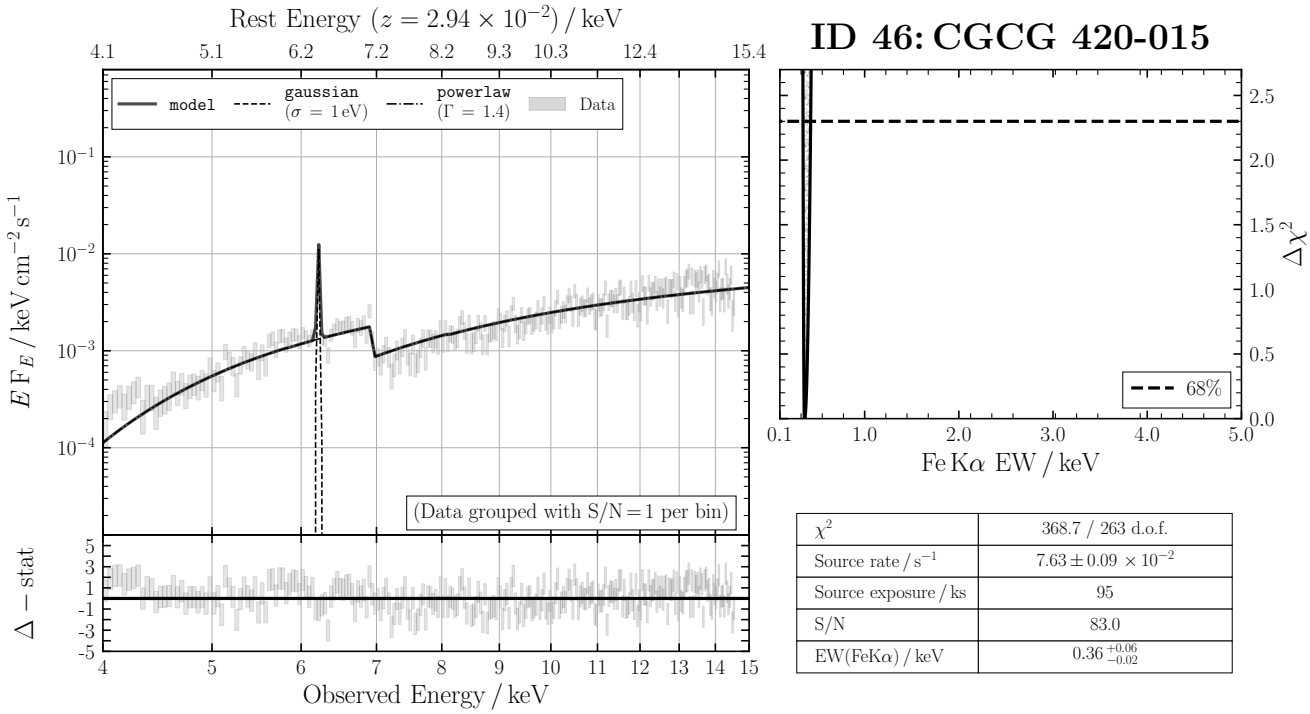

χ^2	368.7 / 263 d.o.f.
Source rate / s^{-1}	$7.63 \pm 0.09 \times 10^{-2}$
Source exposure / ks	95
S/N	83.0
EW(FeKα) / keV	$0.36^{+0.06}_{-0.02}$

Figure B43. ID 46: CGCG 420-015

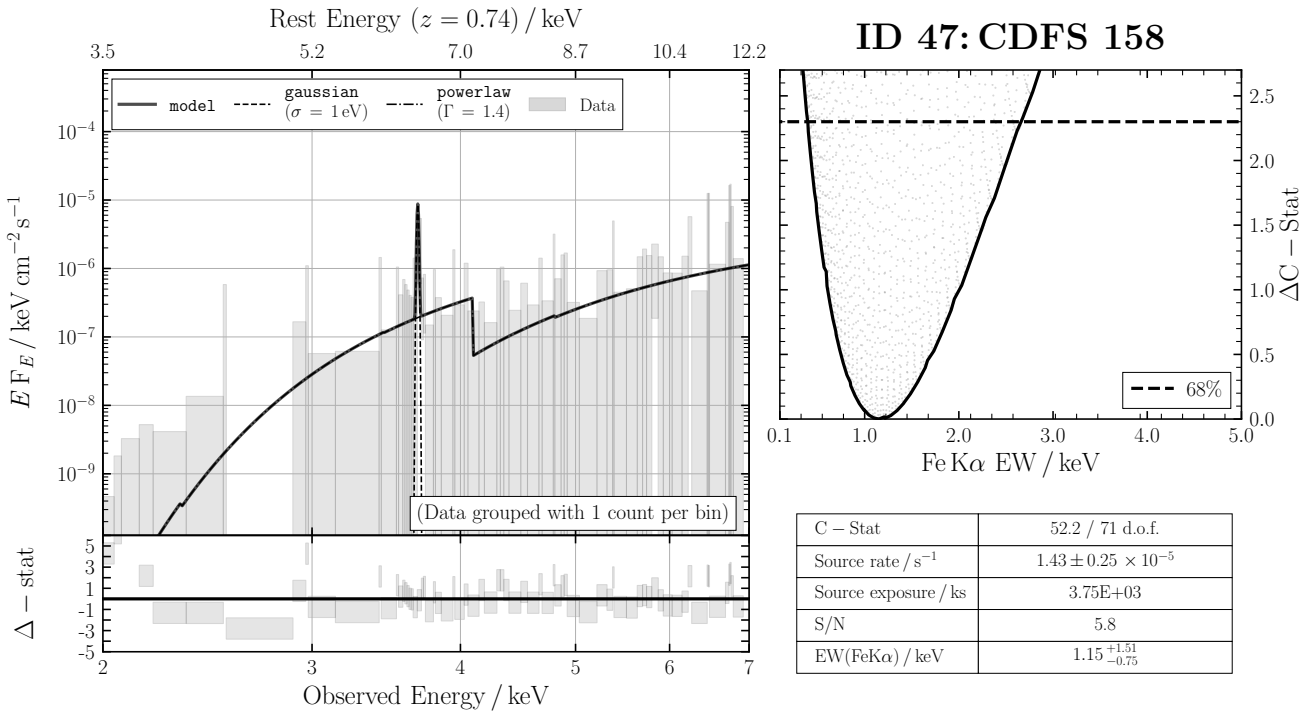

C − Stat	52.2 / 71 d.o.f.
Source rate / s^{-1}	$1.43 \pm 0.25 \times 10^{-5}$
Source exposure / ks	3.75E+03
S/N	5.8
EW(FeKα) / keV	$1.15^{+1.51}_{-0.75}$

Figure B44. ID 47: CDFS 158

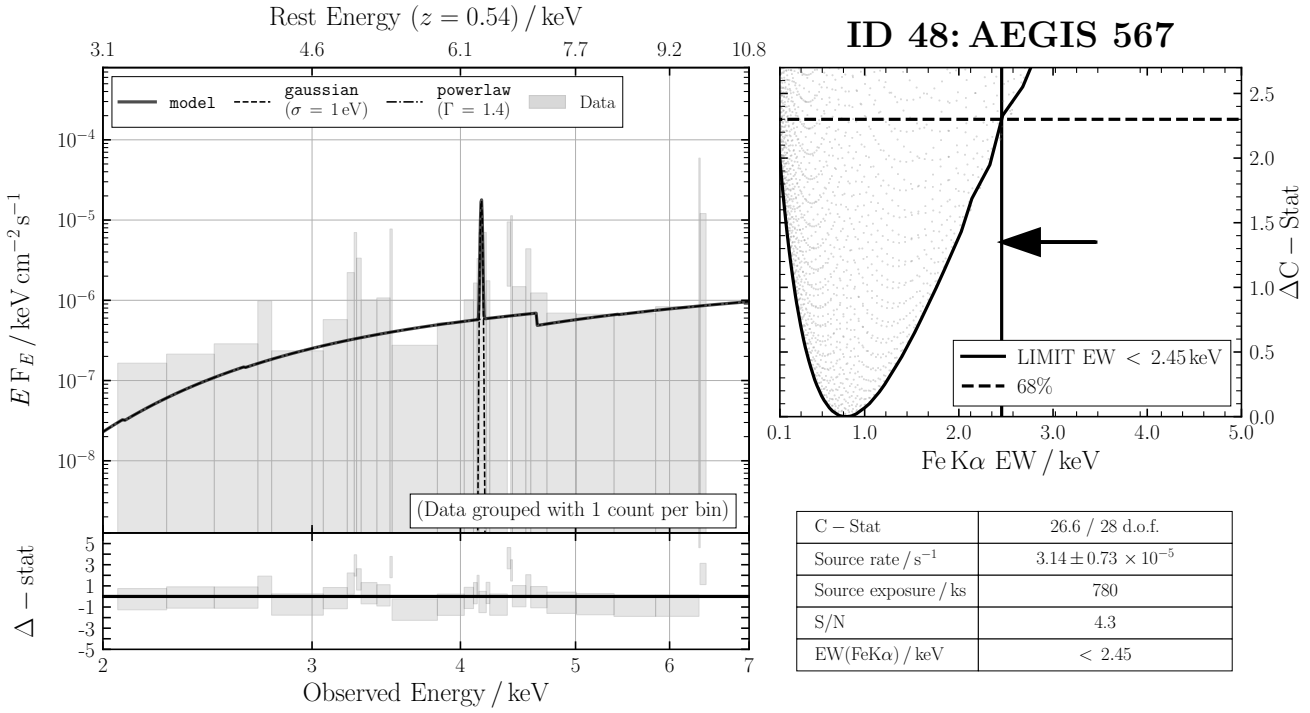

C − Stat	26.6 / 28 d.o.f.
Source rate / s^{-1}	$3.14 \pm 0.73 \times 10^{-5}$
Source exposure / ks	780
S/N	4.3
EW(FeKα) / keV	< 2.45

Figure B45. ID 48: AEGIS 567

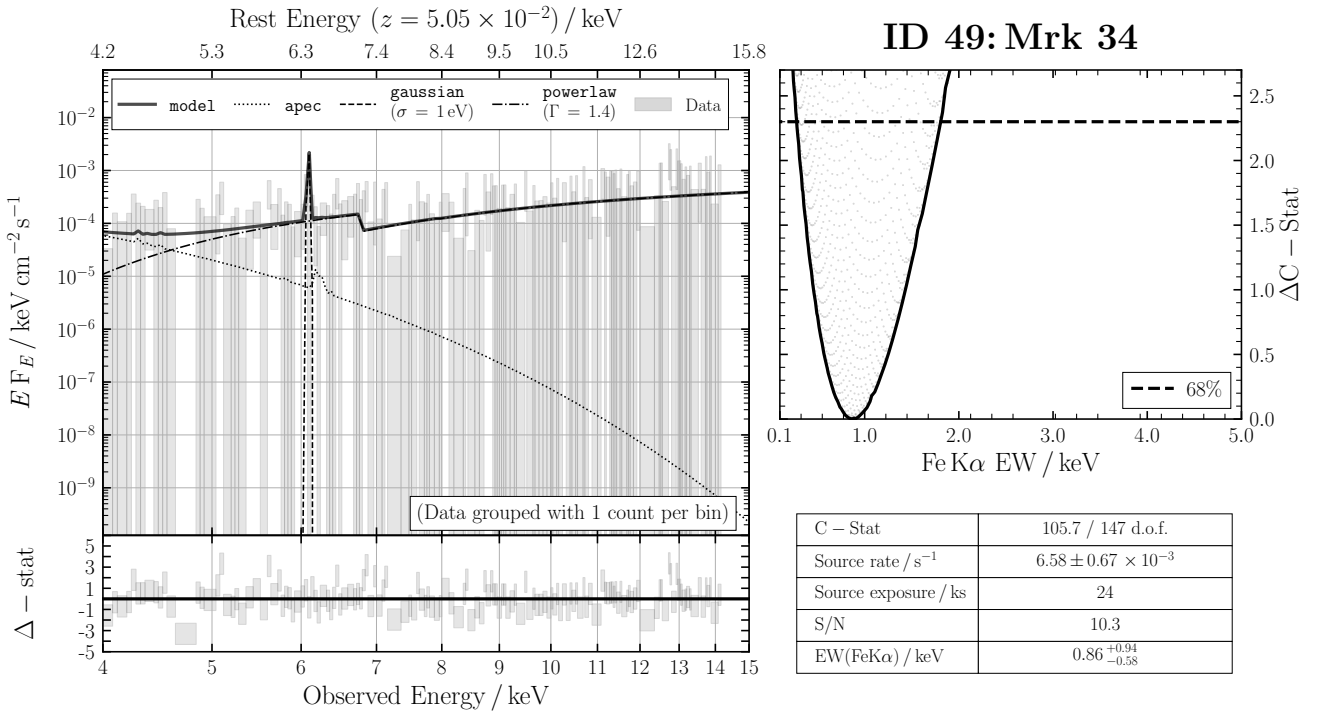

C − Stat	105.7 / 147 d.o.f.
Source rate / s^{-1}	$6.58 \pm 0.67 \times 10^{-3}$
Source exposure / ks	24
S/N	10.3
EW(FeKα) / keV	$0.86^{+0.94}_{-0.58}$

Figure B46. ID 49: Mrk 34

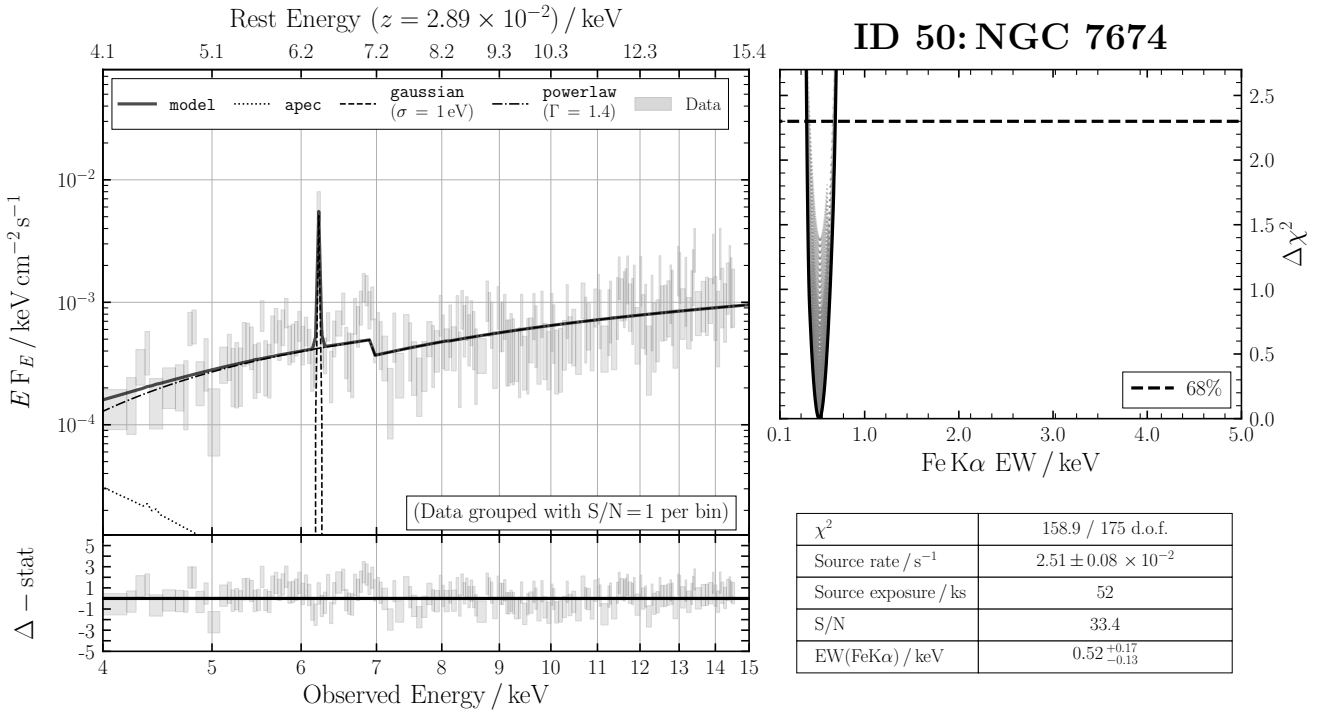

χ^2	158.9 / 175 d.o.f.
Source rate / s^{-1}	$2.51 \pm 0.08 \times 10^{-2}$
Source exposure / ks	52
S/N	33.4
EW(FeKα) / keV	$0.52^{+0.17}_{-0.13}$

Figure B47. ID 50: NGC 7674

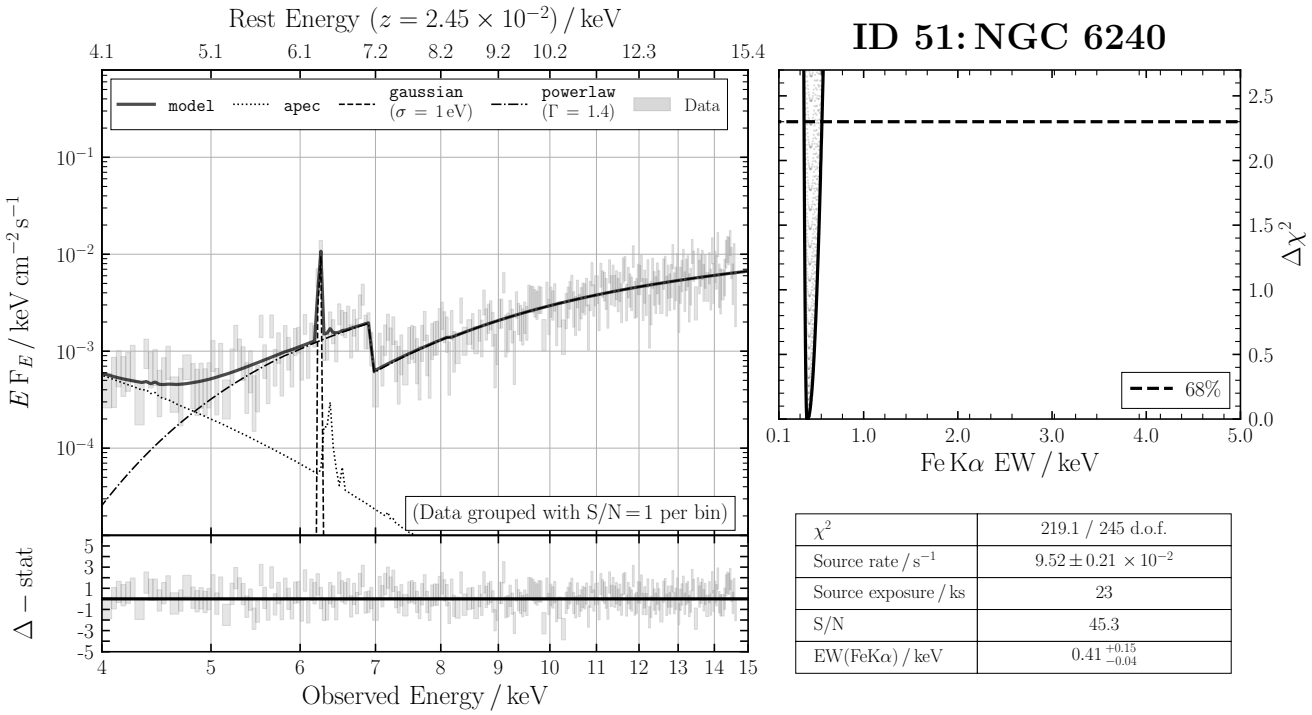

χ^2	219.1 / 245 d.o.f.
Source rate / s^{-1}	$9.52 \pm 0.21 \times 10^{-2}$
Source exposure / ks	23
S/N	45.3
EW(FeKα) / keV	$0.41^{+0.15}_{-0.04}$

Figure B48. ID 51: NGC 6240

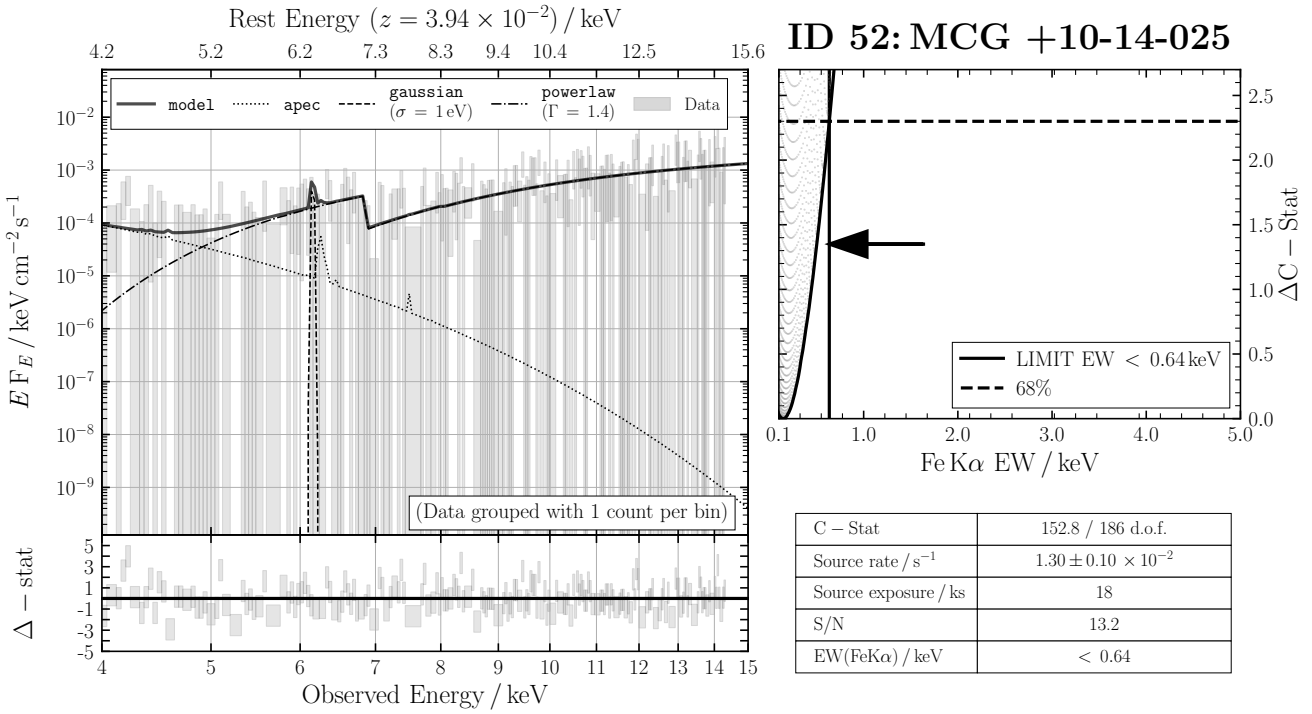

C − Stat	152.8 / 186 d.o.f.
Source rate / s^{-1}	$1.30 \pm 0.10 \times 10^{-2}$
Source exposure / ks	18
S/N	13.2
EW(FeKα) / keV	< 0.64

Figure B49. ID 52: MCG +10-14-025

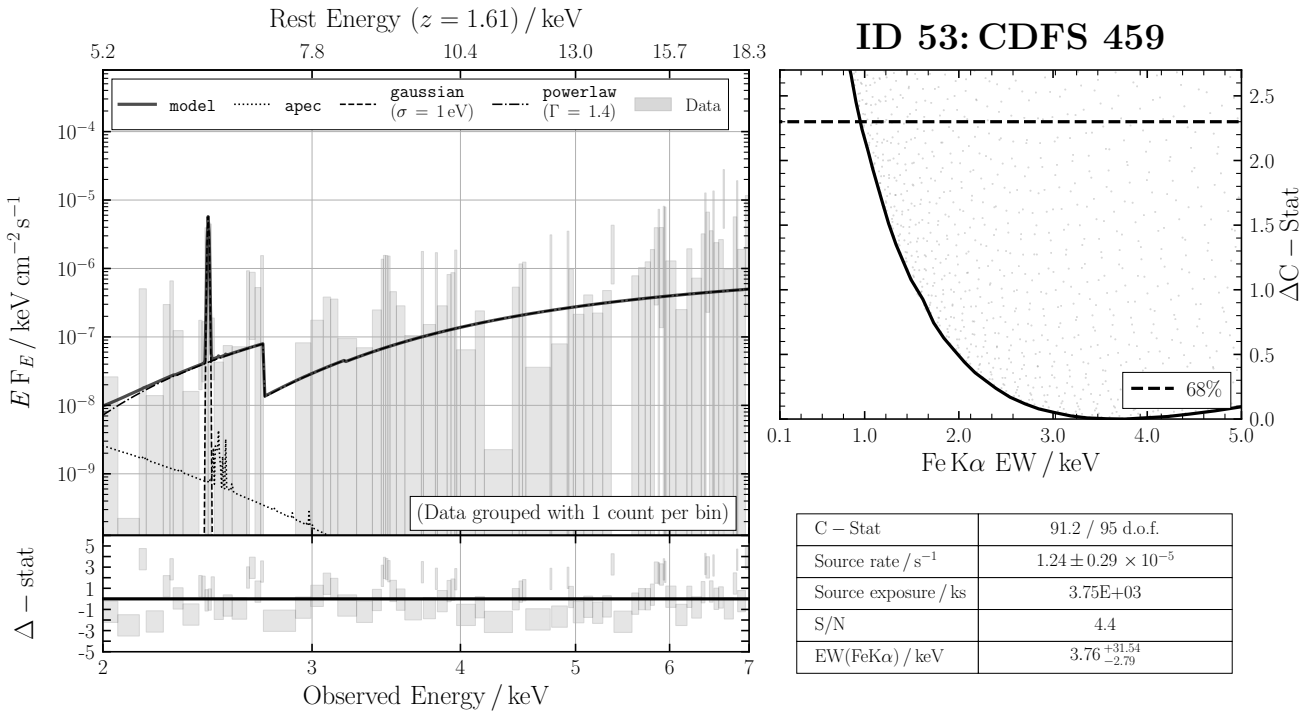

C − Stat	91.2 / 95 d.o.f.
Source rate / s^{-1}	$1.24 \pm 0.29 \times 10^{-5}$
Source exposure / ks	3.75E+03
S/N	4.4
EW(FeKα) / keV	$3.76^{+31.54}_{-2.79}$

Figure B50. ID 53: CDFS 459

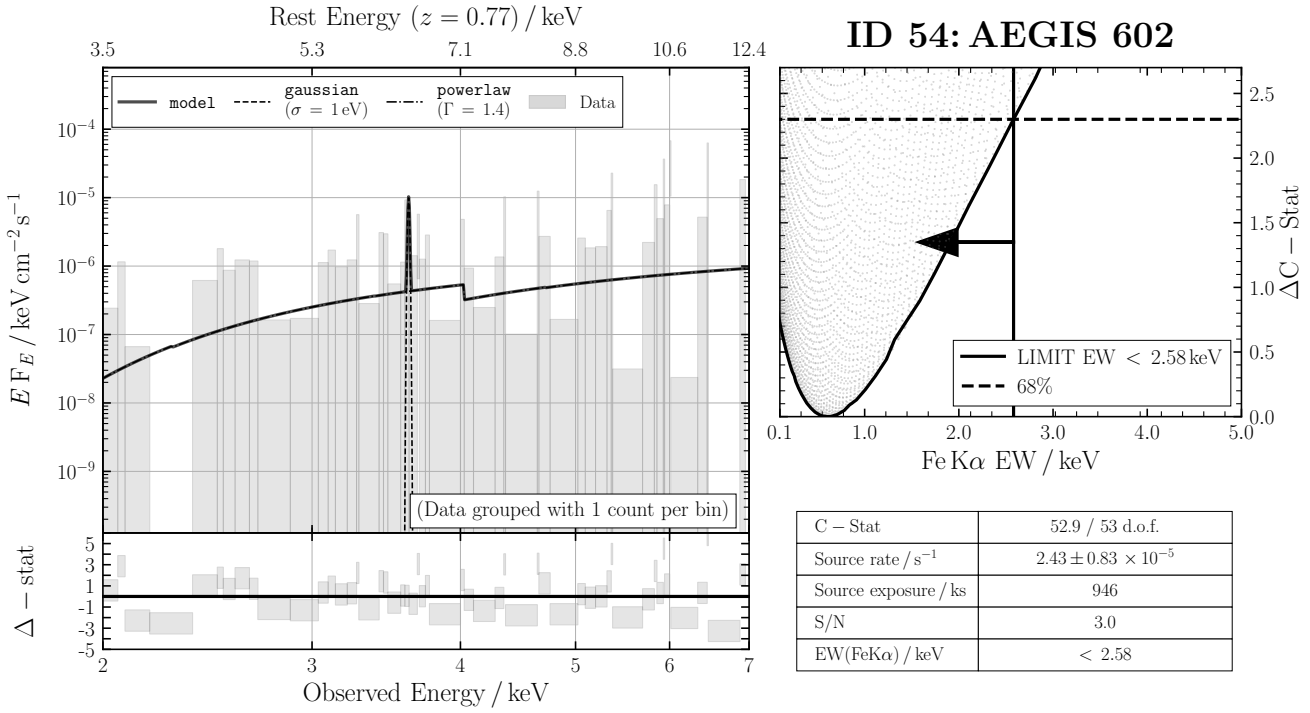

C − Stat	52.9 / 53 d.o.f.
Source rate / s^{-1}	$2.43 \pm 0.83 \times 10^{-5}$
Source exposure / ks	946
S/N	3.0
EW(FeKα) / keV	< 2.58

Figure B51. ID 54: AEGIS 602

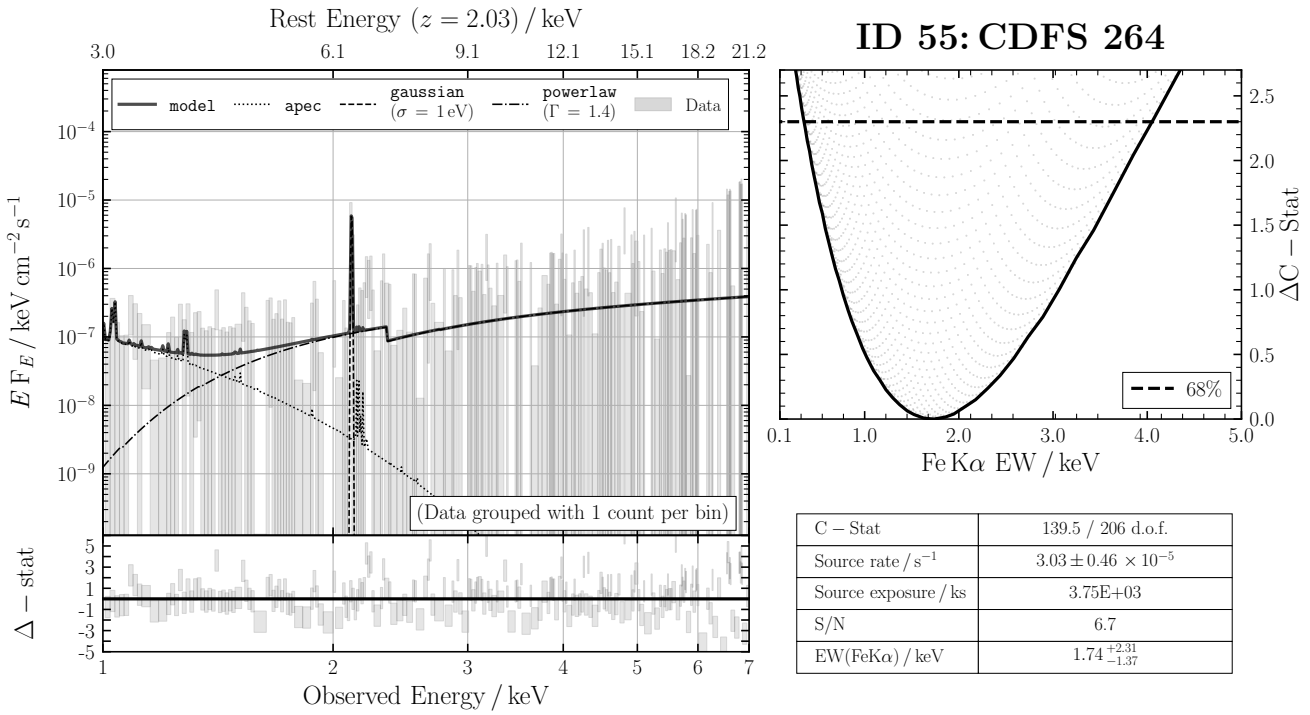

C − Stat	139.5 / 206 d.o.f.
Source rate / s^{-1}	$3.03 \pm 0.46 \times 10^{-5}$
Source exposure / ks	3.75E+03
S/N	6.7
EW(FeKα) / keV	$1.74^{+2.31}_{-1.37}$

Figure B52. ID 55: CDFS 264

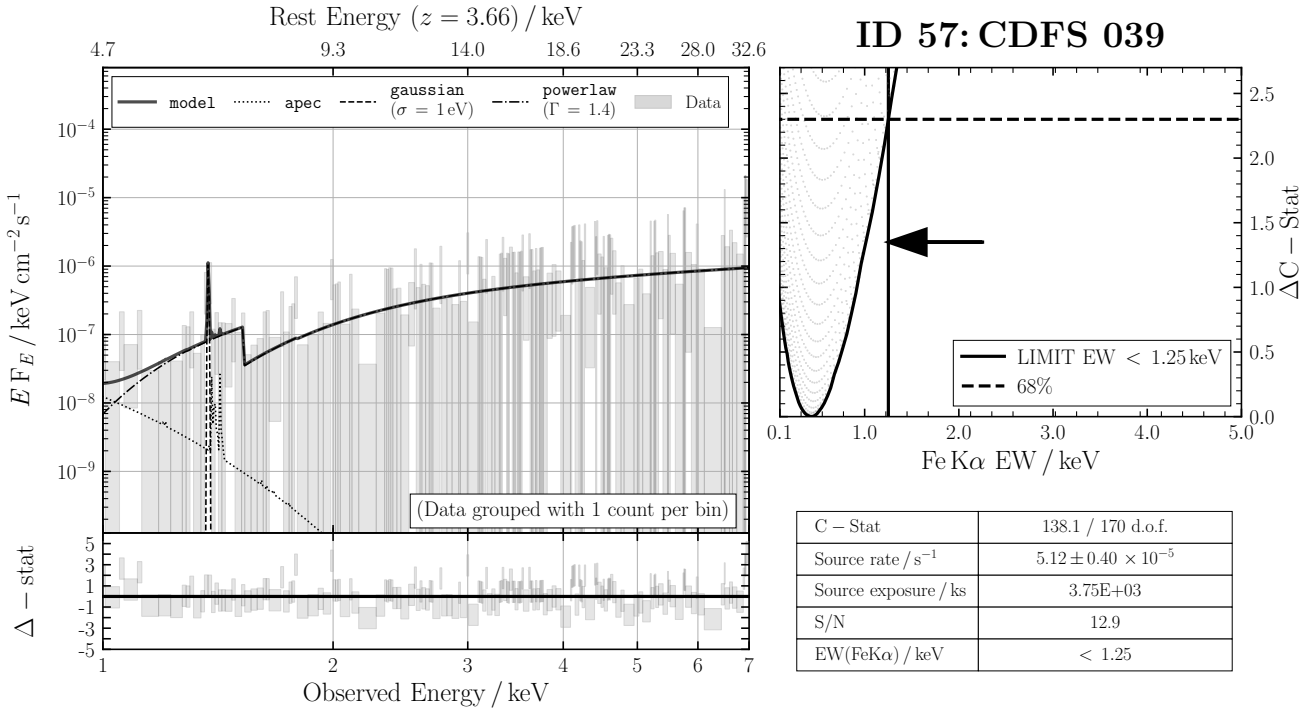

C − Stat	138.1 / 170 d.o.f.
Source rate / s^{-1}	$5.12 \pm 0.40 \times 10^{-5}$
Source exposure / ks	3.75E+03
S/N	12.9
EW(FeKα) / keV	< 1.25

Figure B53. ID 57: CDFS 039

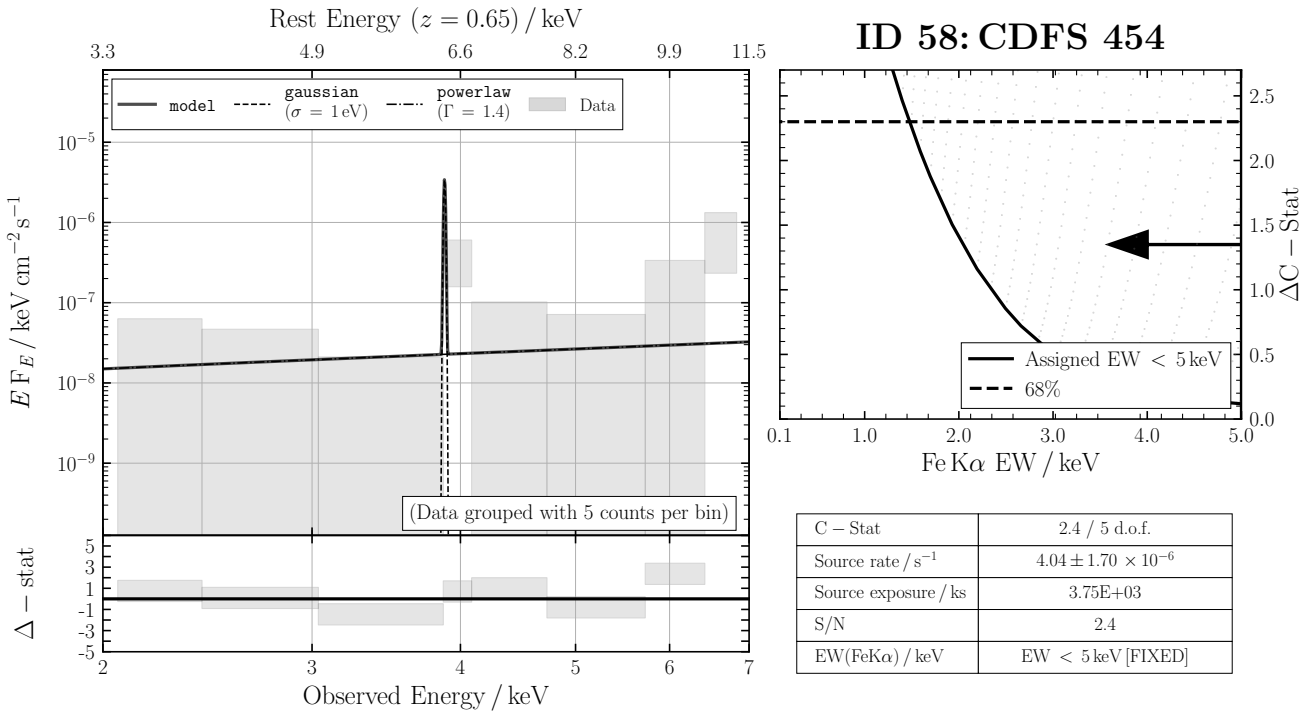

C − Stat	2.4 / 5 d.o.f.
Source rate / s^{-1}	$4.04 \pm 1.70 \times 10^{-6}$
Source exposure / ks	3.75E+03
S/N	2.4
EW(FeKα) / keV	EW < 5 keV [FIXED]

Figure B54. ID 58: CDFS 454

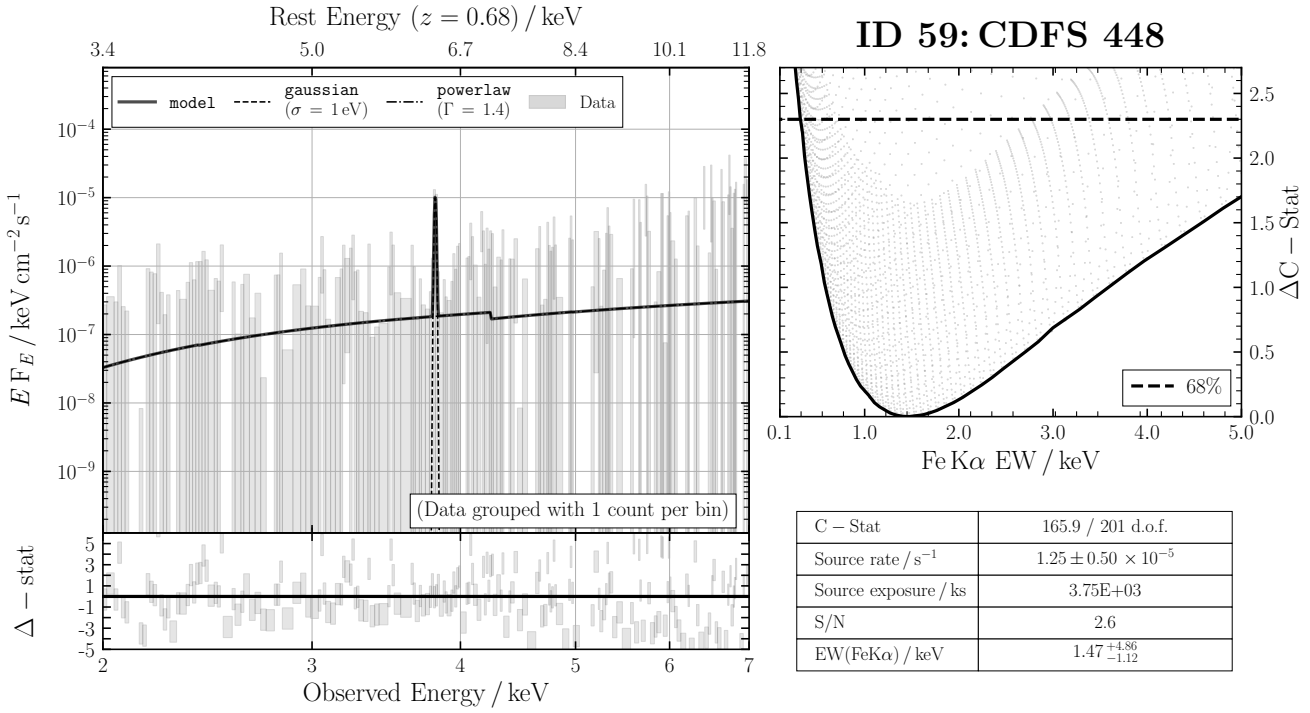

C − Stat	165.9 / 201 d.o.f.
Source rate / s^{-1}	$1.25 \pm 0.50 \times 10^{-5}$
Source exposure / ks	3.75E+03
S/N	2.6
EW(FeKα) / keV	$1.47^{+4.86}_{-1.12}$

Figure B55. ID 59: CDFS 448

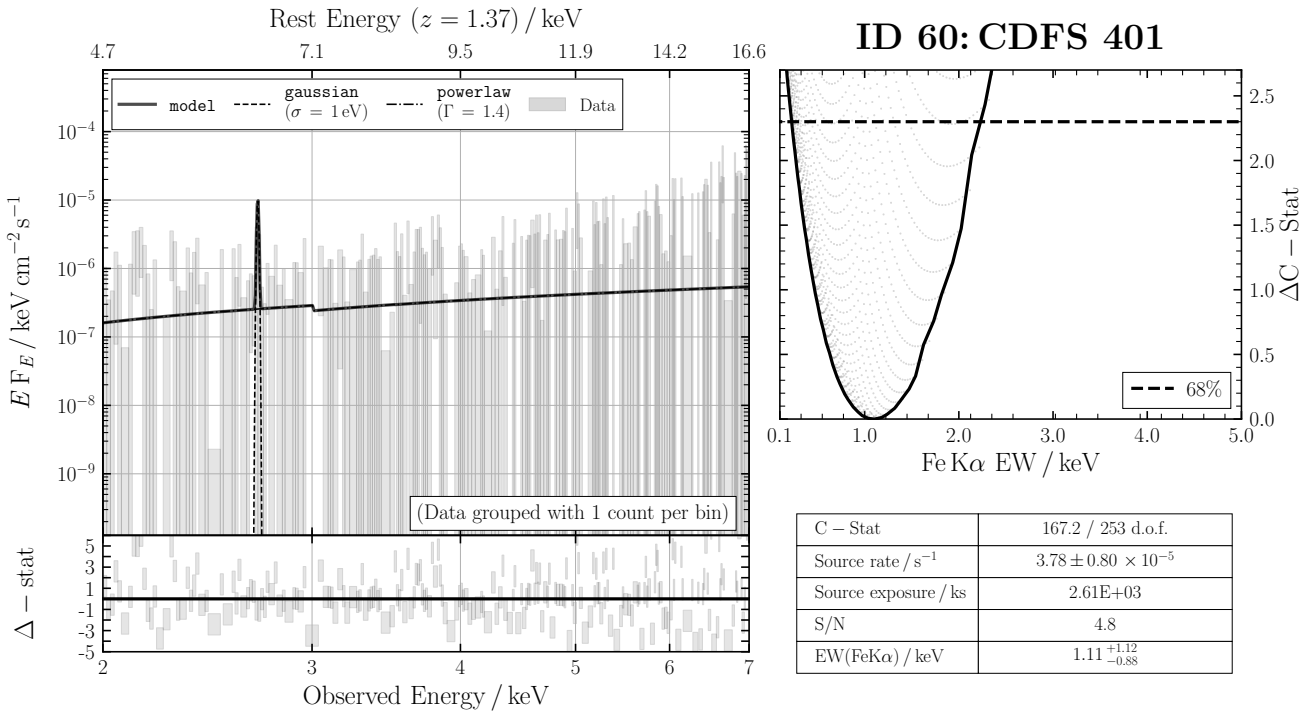

C − Stat	167.2 / 253 d.o.f.
Source rate / s^{-1}	$3.78 \pm 0.80 \times 10^{-5}$
Source exposure / ks	2.61E+03
S/N	4.8
EW(FeKα) / keV	$1.11^{+1.12}_{-0.88}$

Figure B56. ID 60: CDFS 401

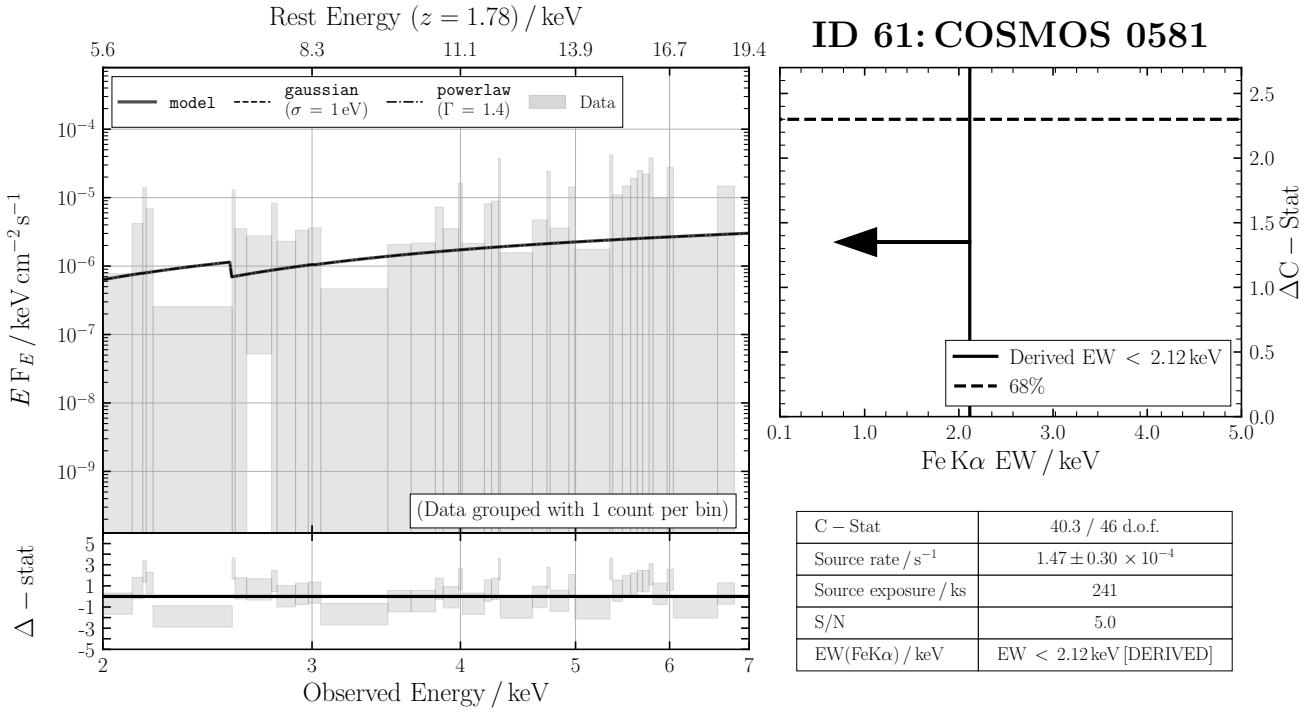

C − Stat	40.3 / 46 d.o.f.
Source rate / s^{-1}	$1.47 \pm 0.30 \times 10^{-4}$
Source exposure / ks	241
S/N	5.0
EW(FeKα) / keV	EW < 2.12 keV [DERIVED]

Figure B57. ID 61: COSMOS 0581

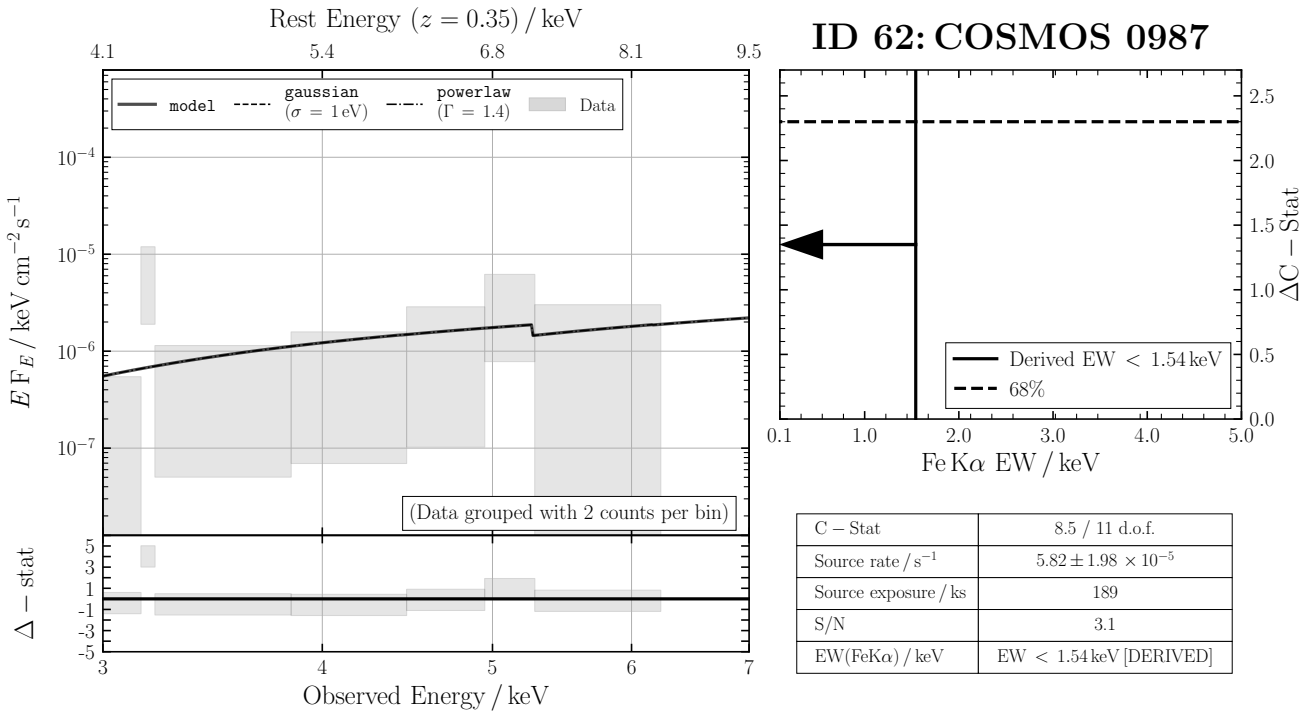

C − Stat	8.5 / 11 d.o.f.
Source rate / s^{-1}	$5.82 \pm 1.98 \times 10^{-5}$
Source exposure / ks	189
S/N	3.1
EW(FeKα) / keV	EW < 1.54 keV [DERIVED]

Figure B58. ID 62: COSMOS 0987

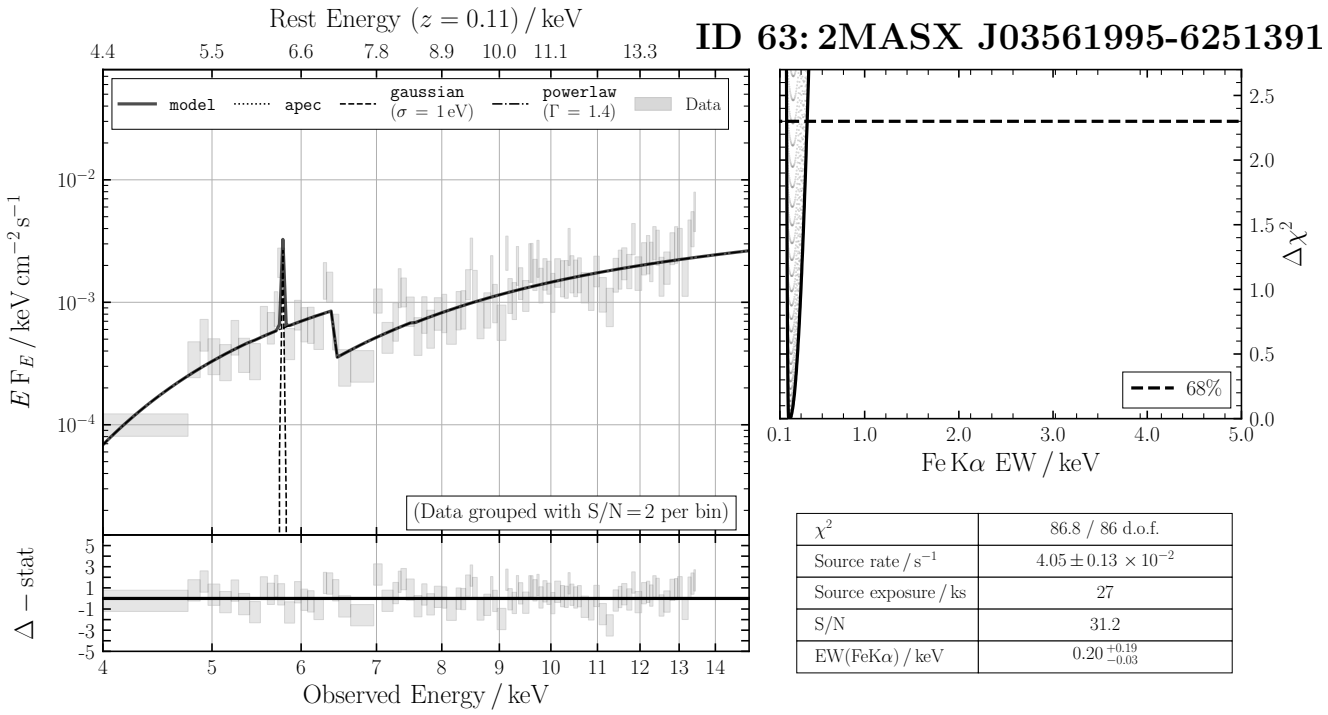

χ^2	86.8 / 86 d.o.f.
Source rate / s^{-1}	$4.05 \pm 0.13 \times 10^{-2}$
Source exposure / ks	27
S/N	31.2
EW(FeKα) / keV	$0.20^{+0.19}_{-0.03}$

Figure B59. ID 63: 2MASX J03561995-6251391

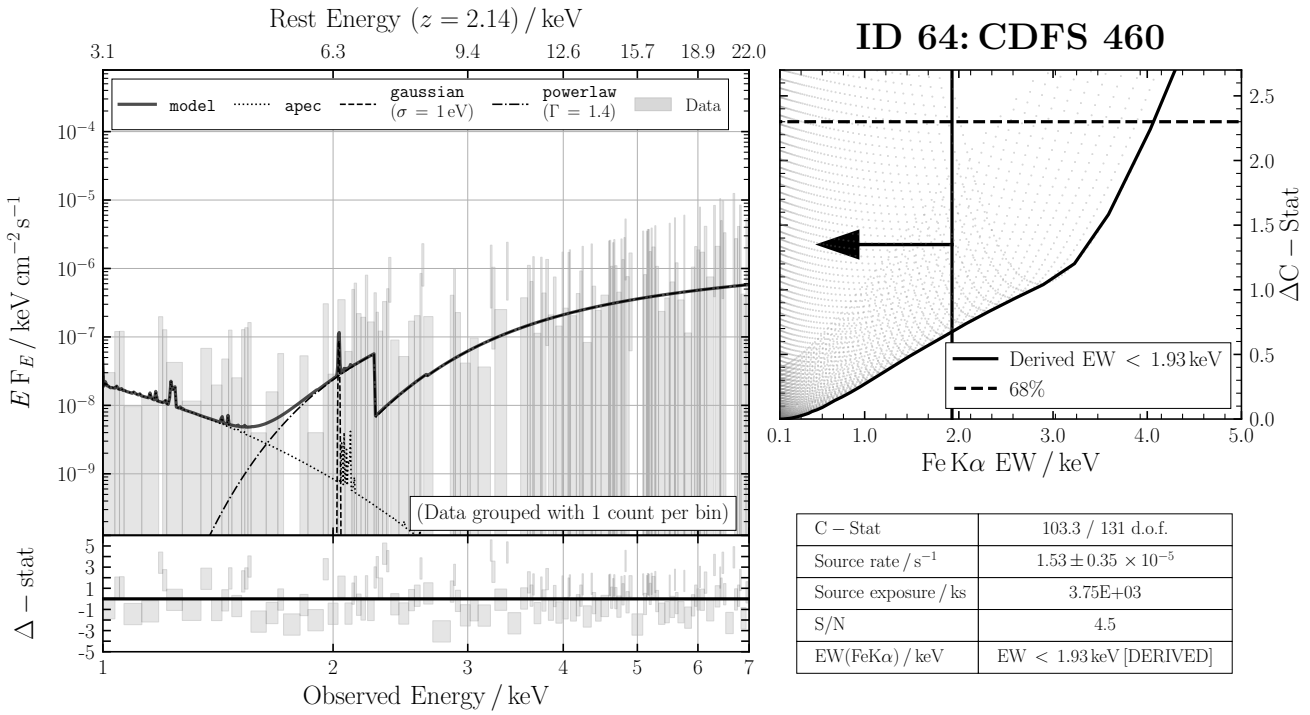

C − Stat	103.3 / 131 d.o.f.
Source rate / s^{-1}	$1.53 \pm 0.35 \times 10^{-5}$
Source exposure / ks	3.75E+03
S/N	4.5
EW(FeKα) / keV	EW < 1.93 keV [DERIVED]

Figure B60. ID 64: CDFS 460

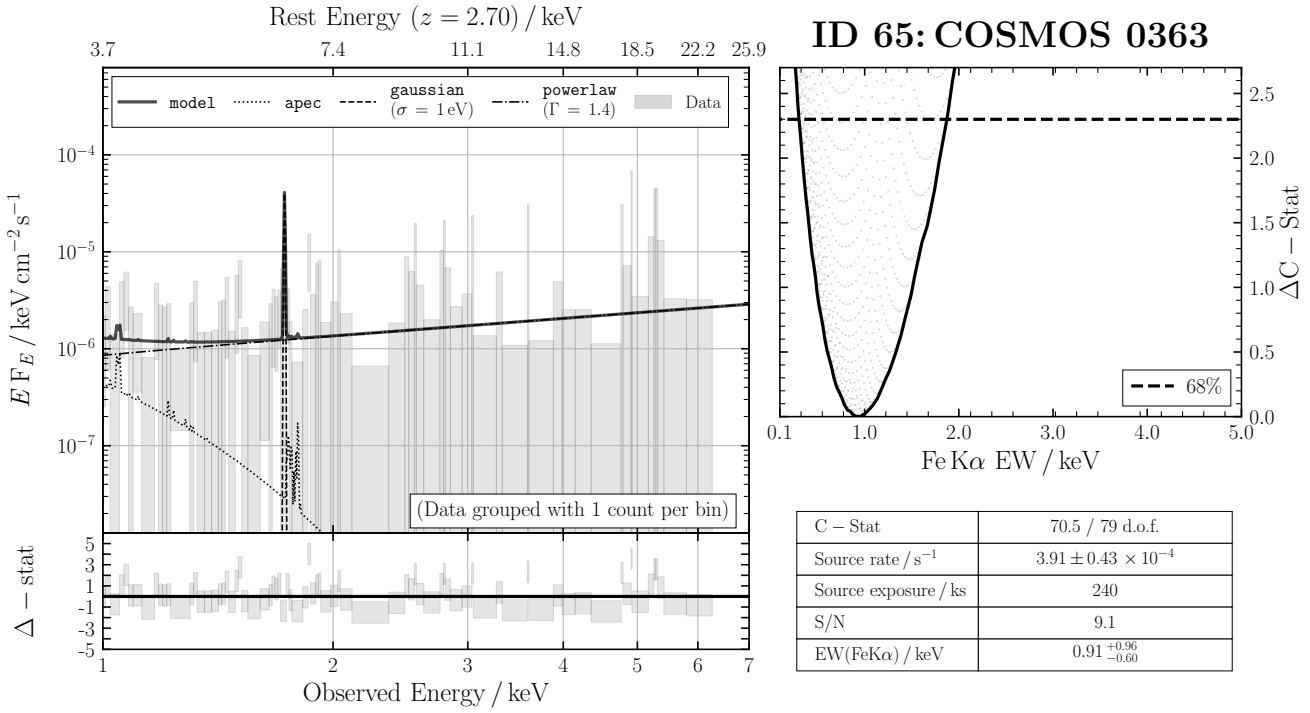

C − Stat	70.5 / 79 d.o.f.
Source rate / s^{-1}	$3.91 \pm 0.43 \times 10^{-4}$
Source exposure / ks	240
S/N	9.1
EW(FeKα) / keV	$0.91\,^{+0.96}_{-0.60}$

Figure B61. ID 65: COSMOS 0363

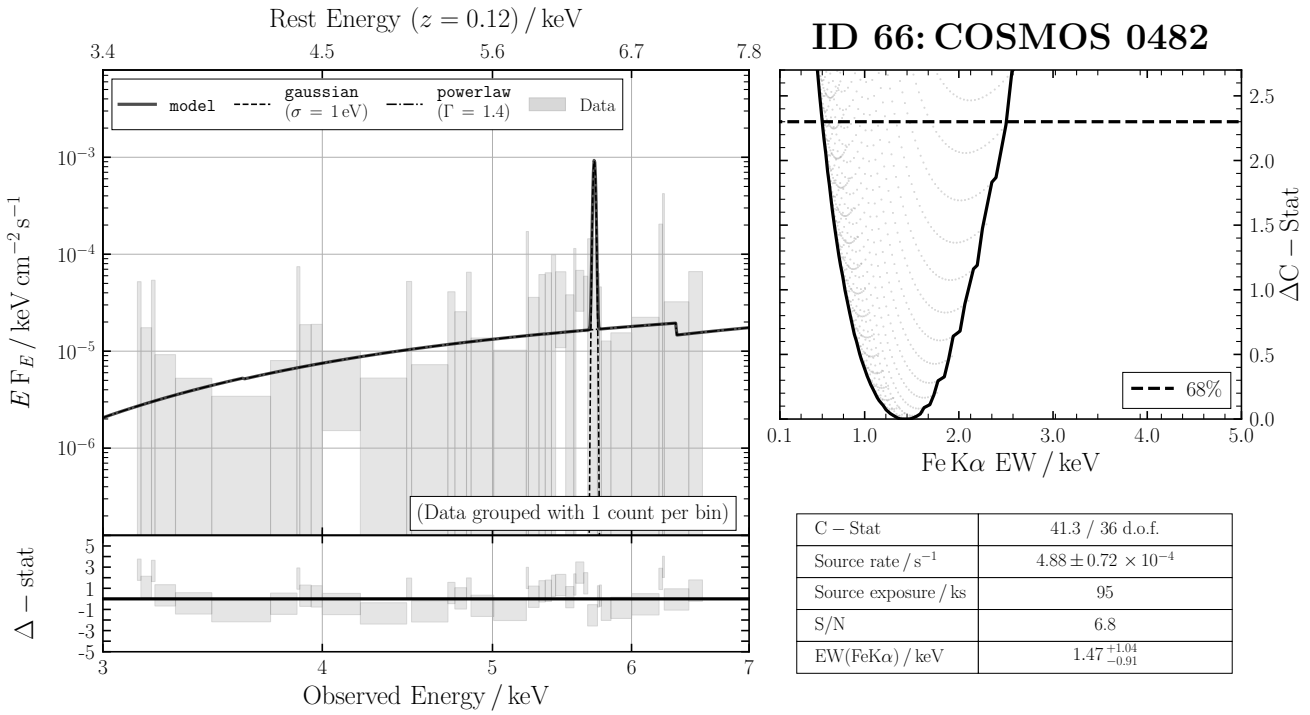

C − Stat	41.3 / 36 d.o.f.
Source rate / s^{-1}	$4.88 \pm 0.72 \times 10^{-4}$
Source exposure / ks	95
S/N	6.8
EW(FeKα) / keV	$1.47^{+1.04}_{-0.91}$

Figure B62. ID 66: COSMOS 0482

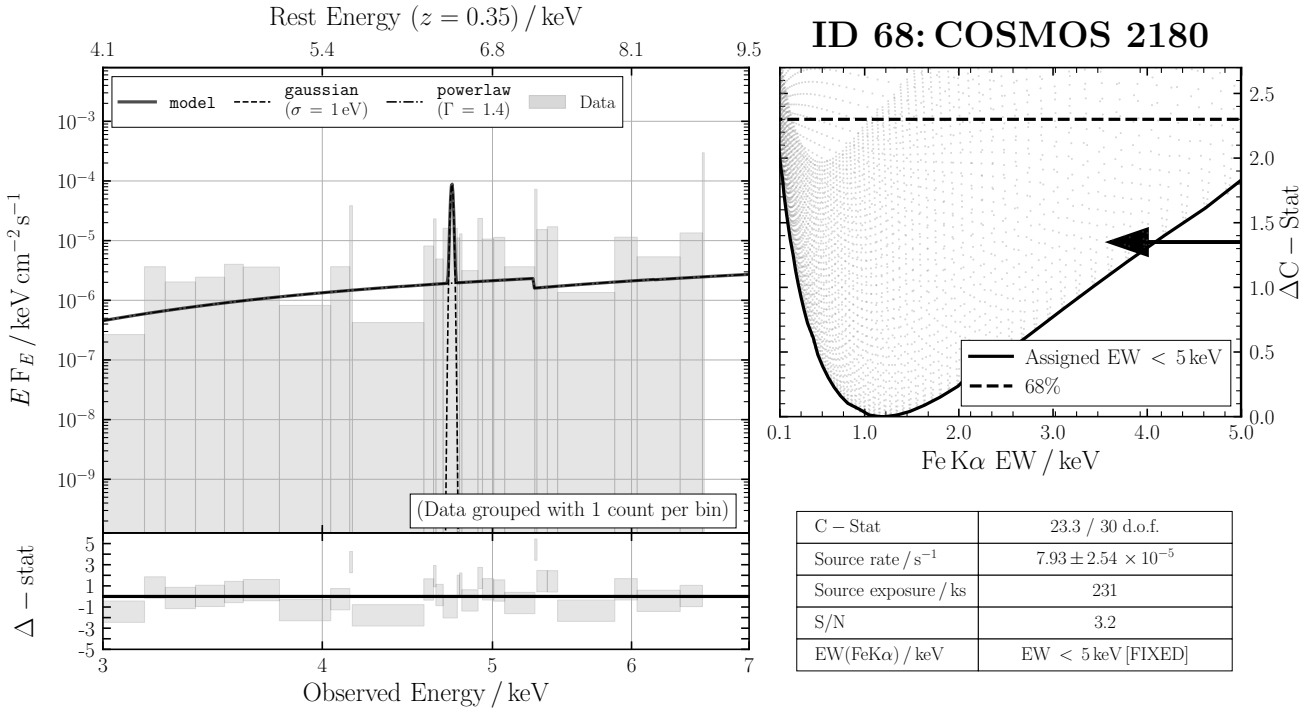

C − Stat	23.3 / 30 d.o.f.
Source rate / s^{-1}	$7.93 \pm 2.54 \times 10^{-5}$
Source exposure / ks	231
S/N	3.2
EW(FeKα) / keV	EW < 5 keV [FIXED]

Figure B63. ID 68: COSMOS 2180

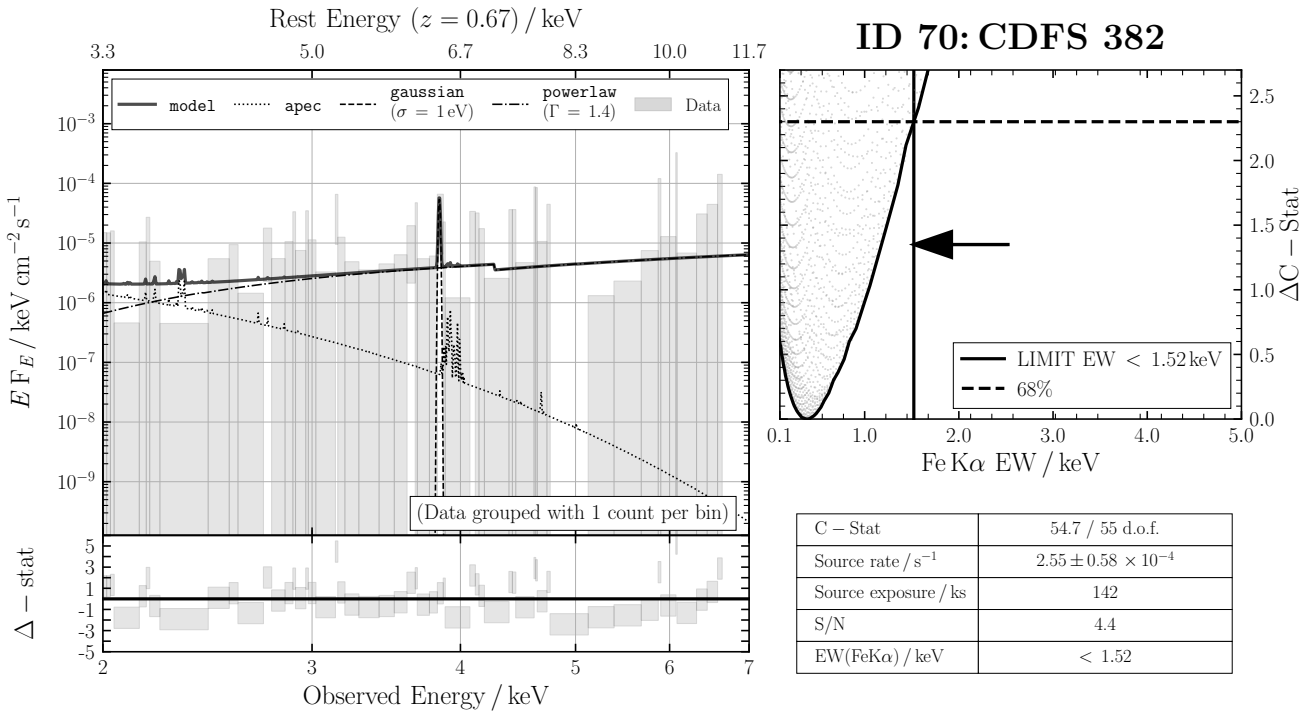

C − Stat	54.7 / 55 d.o.f.
Source rate / s^{-1}	$2.55 \pm 0.58 \times 10^{-4}$
Source exposure / ks	142
S/N	4.4
EW(FeKα) / keV	< 1.52

Figure B64. ID 70: CDFS 382

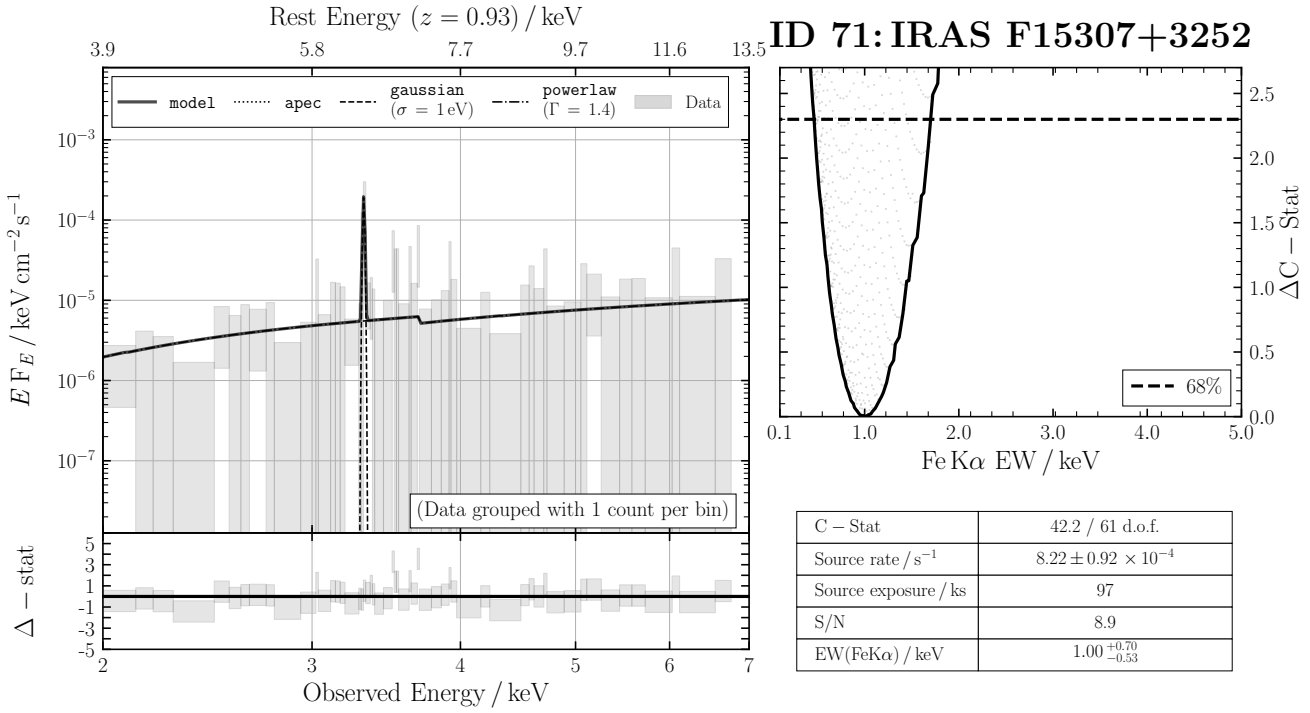

C − Stat	42.2 / 61 d.o.f.
Source rate / s^{-1}	$8.22 \pm 0.92 \times 10^{-4}$
Source exposure / ks	97
S/N	8.9
EW(FeKα) / keV	$1.00^{+0.70}_{-0.53}$

Figure B65. ID 71: IRAS F15307+3252